CHAPTER IV
RESULTS AND DISCUSSION

The pyrolysis of waste tire produces gas, liquid, and solid products. Especially, the gas product with valuable fractions such as light olefins can be produced. All of these products can be used as petrochemical feedstock and a fuel source. Since, catalytic pyrolysis is the way to improve the quality and quantity of desired products. In this research, in order to develop a commercial Ru/HMOR catalyst for the pyrolysis of waste tire, its optimum composition, pellet size, and deactivation were studied. The results and discussions are presented as follows.

4.1 Determination of the optimum composition of a commercial Ru/HMOR-based catalyst

The optimum composition of a being-developed commercial Ru/HMOR catalyst for light olefins production from the catalytic pyrolysis of tire was investigated. The pure, active Ru/HMOR zeolite, kaolin (a matrix), and α-alumina (a binder) were also examined as a reference. The optimum composition of catalyst was determined by varying %wt of Ru/HMOR zeolite (active ingredient) from 20–50%wt and kaolin from 40–70%wt at a fixed 10%wt of α-alumina, as displayed in Table 4.1.

4.1.1 Catalyst characterization

Table 4.1 summarizes the physical and chemical properties of the studied Ru/HMOR-based catalysts. The surface area, pore volume, and pore size of the catalysts were measured by using the BET method. And, the surface area and pore volume of the studied catalysts are slightly increased with the increasing active Ru/HMOR. However, they are lower than those of the active Ru/HMOR zeolite.

Moreover, the pore size distribution is shown in Figure 4.1. The pore size diameters of the Ru/HMOR-based catalysts are higher than that of the active Ru/HMOR zeolite, possibly caused by the physical mixing of all components.

Table 4.1 Physical and chemical properties of the studied Ru/HMOR-based catalysts

Catalyst	Composition (%wt)			Pore volume (cm^3/g)	Surface area (m^2/g)
	Ru/HMOR	Kaolin	α-alumina		
Ru/HMOR	100			1.05	437.2
Kaolin		100		0.16	32.87
α-alumina			100	0.48	73.34
BC-20	20	70	10	0.29	112.7
BC-30	30	60	10	0.45	183.7
BC-40	40	50	10	0.58	251.6
BC-50	50	40	10	0.67	289.0

* BC—a being-developed commercial Ru/HMOR-based catalyst

The XRD patterns of the studied catalysts are shown in Figure 4.2. These patterns indicate that the combination of Ru/HMOR with kaolin and α-alumina does not affect the structure of each component. So, no chemical bonds are formed between the Ru/HMOR and kaolin. However, due to the low amount of metal loaded on the catalysts, the signal for metallic ruthenium has a very small intensity at $2\theta = 44^{\circ}$.

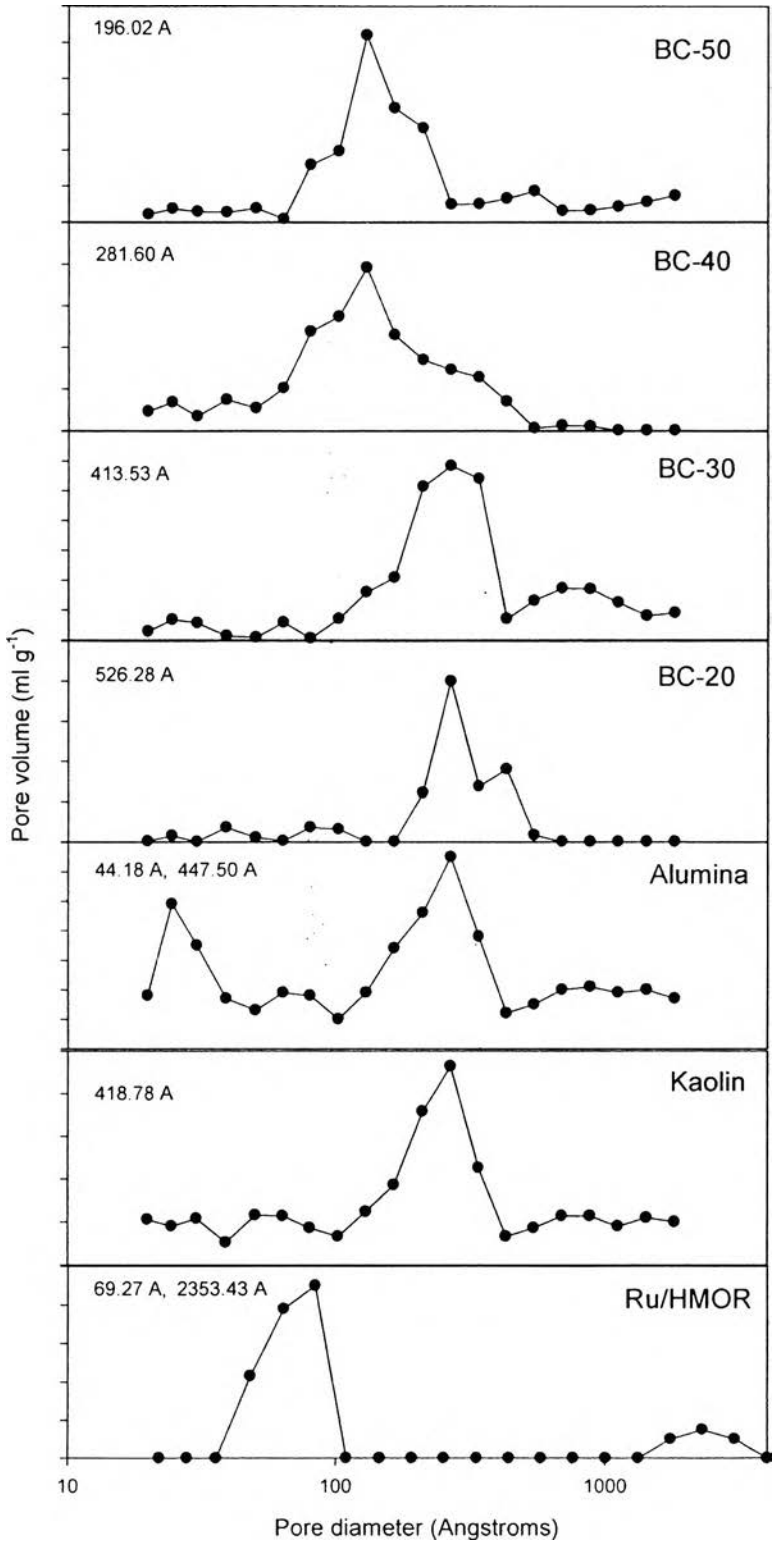

Figure 4.1 Variation of the pore size distribution of the studied Ru/HMOR-based catalysts and each separate component.

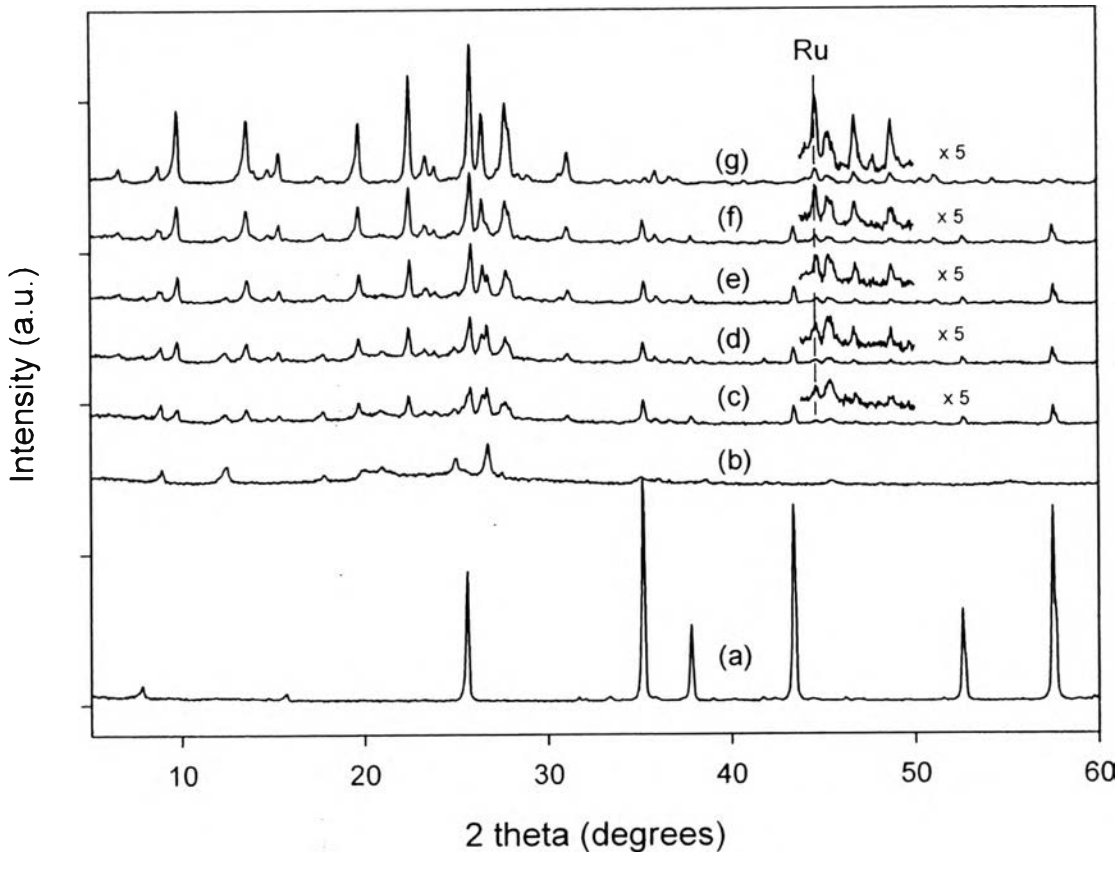

Figure 4.2 The XRD patterns of: (a) α-alumina, (b) kaolin, (c) BC-20, (d) BC-30, (e) BC-40, (f) BC-50, and (g) Ru/HMOR.

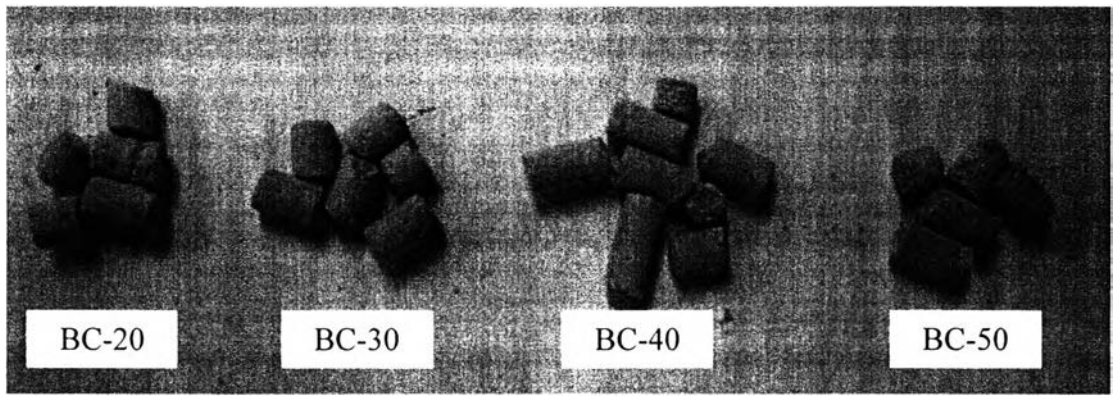

Figure 4.3 An appearance of the studied Ru/HMOR-based catalysts with various compositions.

4.1.2 Product Distribution

The products of tire pyrolysis are distributed into gas, liquid, and solid, which are presented in Figure 4.4.

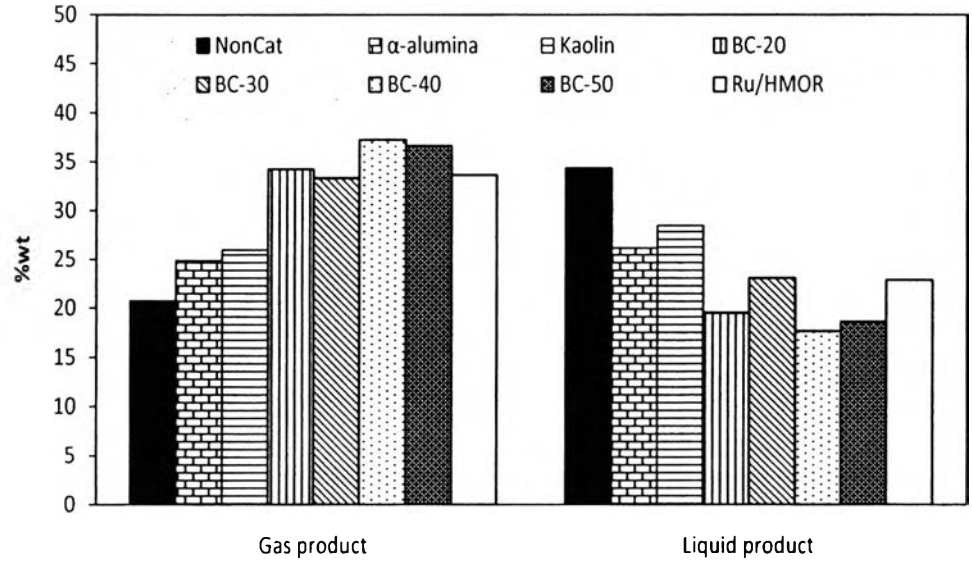

Figure 4.4 Product distributions from the catalytic pyrolysis of scrap tire using the Ru/HMOR-based catalysts with various compositions.

The figure shows the effect of the Ru/HMOR-based catalysts on the pyrolysis products. The results show that all the studied Ru/HMOR-based catalysts including the active Ru/HMOR zeolite have the influence on the product yields, in which they increase the gas yield by about 15%wt, and consequently decrease the liquid yields as compared to the non-catalytic case at the same conditions. This is because the bifunctional catalyst (Ru/HMOR) has the higher cracking activity, which can crack liquid products or heavy hydrocarbon molecules into light hydrocarbon molecules or the gaseous products. Similarly, Kittikom, 2008 reported that ruthenium loaded on the zeolite can increase thermal cracking activity.

For comparison among the studied Ru/HMOR-based catalysts, it was found that the increasing amount of the active Ru/HMOR blended in the catalysts affected significantly to the gas yield. It might be due to the effect of matrix in the catalysts. Furthermore, the solid yields for both catalytic and non-catalytic cases remain constant at around 45.3 %wt by average. This is because that the tire was completely cracked at 500°C (Nguyễn *et al.*, 2009).

4.1.3 Gas Yield

The pyrolysis gas is comprised of methane, ethane, ethylene, propane, propylene, mixed-C_4, mixed-C_5, mixed-C_6, mixed-C_7, and mixed-C_8 hydrocarbons as shown in Figure 4.5. The results show that the studied Ru/HMOR-based catalysts and the active Ru/HMOR zeolite exhibit the light gas products such as ethylene, ethane, propylene, and propane increase as much as obtained from non-catalytic cases. It is because of the bifunctional catalyst (Ru/HMOR), which have two distinct catalytic sites. The first site is metal sites (Ru) which can drive the hydrogenation and/or dehydrogenation reaction (Eq.(1)). And, Ru-based catalyst also occur the hydrogenolysis reaction (Nguyễn *et al.*, 2009). The second site is acid sites (HMOR) which protonate hydrocarbons, leading to the carbenium ions formation, which subsequently go through isomerization, cracking (β-scission, Eq.(2)), and alkylation (Hongbin *et al.*, 2005). So, the pathway can produce light gas hydrocarbon as shown below as an example.

$$\text{Alkane} \xrightleftharpoons{Ru} \text{alkene} + \text{hydrogen} \qquad (1)$$

$$\text{Alkene} \xrightleftharpoons{+H^+} \text{carbenium ions} \xrightleftharpoons{\beta\text{-scission}} \text{olefin} + \text{new carbenium ion} \qquad (2)$$

Similarly, Shiraga *et al.* (2007) studied the partial oxidation of propane. And, they suggested that ruthenium metal catalyzed the cracking of propane resulting in high selectivity to C_2-C_3 compounds and also to CH_4. However, among the studied BC catalysts, the yields of light gas are insignificantly different although the catalysts consist of significantly different amounts of active Ru/HMOR.

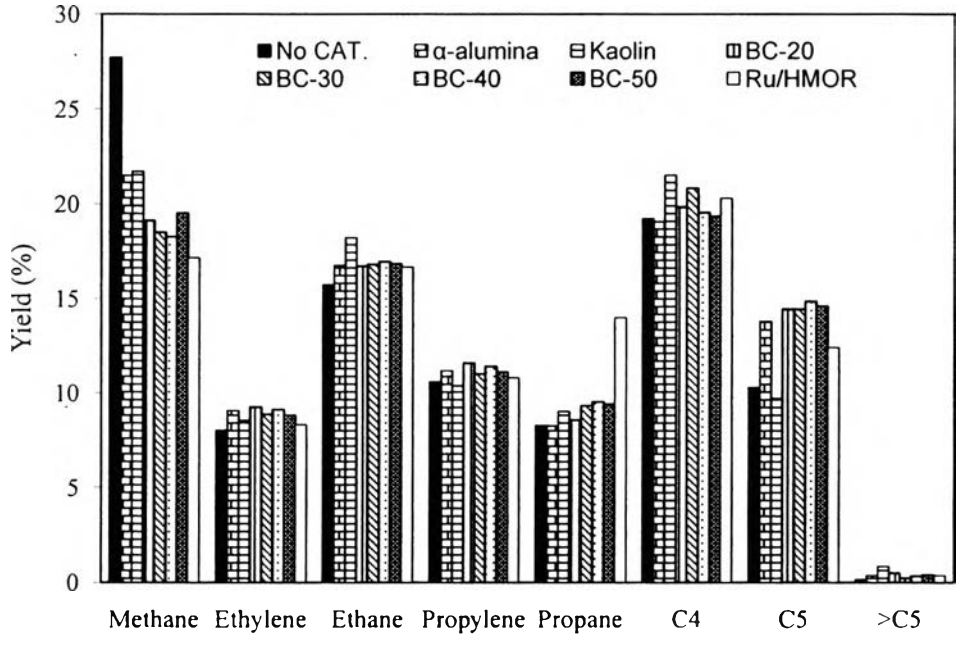

Figure 4.5 Gas compositions from the catalytic pyrolysis of scrap tire using the Ru/HMOR-based catalysts with various compositions.

4.1.4 Light Olefins Production

Light olefins are widely used as raw materials in petrochemical industries. Conventionally, light olefins can be produced by the stream cracking of paraffinic hydrocarbon (e.g. naphtha) and the fluid catalytic cracking of heavy oils

(heavy gas oil or vacuum gas oil). In this work, the light olefins particularly mean ethylene and propylene in the gas product. The yield on light olefins production per kilogram of waste tire is shown in Figure 4.6.

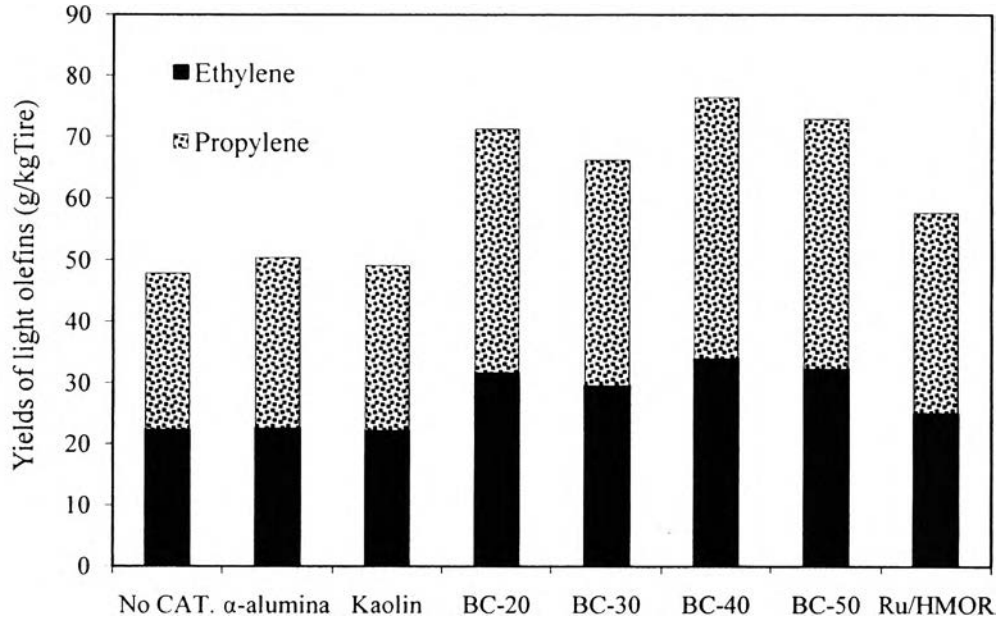

Figure 4.6 Light olefins production from the catalytic pyrolysis of scrap tire using the Ru/HMOR-based catalysts with various compositions.

Figure 4.6 presents that the yields of light olefins per kg of waste tire from using the BC catalysts with various compositions are insignificantly different. However, the studied catalysts have a higher ability to produce the light olefins as compared to the active Ru/HMOR zeolite. This might be because the matrix, which has some effect in the catalyst. This is because of the matrix function. The major function of the matrix is to support the zeolite particles and also to form a diffusion medium for the hydrocarbon molecules. The matrix surrounding the zeolite acts as a heat carrier helping heat transfer or heat dissipation during cracking reaction (Subhash, 1946). The zeolites can exhibit the uncommon property of contracting on heating (i.e. negative thermal expansion) (Lightfoot *et al.*, 2001). The framework structure of zeolite is also linked to the occurrence of low thermal conductivity (Kennedy

and White, 2005). However, the matrix can be used to achieve a monolithic structure. This structure shows highly improved thermal conductivity over that of zeolite alone (Llett *et al.*, 2008). The thermal conductivity is presented in Table 4.2. In addition, the catalytic cracking reaction through the beta scission of carbenium ions at the acid site of a zeolite is an exothermic reaction (Wang *et al.*, 2008). The beta scission of carbenium ion produces an olefins and a new cabenium ion. If the catalyst had contained only the active Ru/HMOR zeolite, good heat distribution by the matrix surrounding would have not occurred during the catalytic cracking reaction, leading to a hotspot and consequently the over-cracking of olefins at the zeolite active sites. With the fact that the primary carbeniun ion is the least stable, the hydrocarbon molecules formed by catalytic cracking should contain at least three carbon atoms. This fact results in a high production of C3 and C4 from the catalytic cracking reaction. Since no significance on the light olefins yields per weight of tire was found, the light olefins yield per kilogram of tire and gram of active Ru/HMOR is compared as shown in Figure 4.7. It is found that the BC-20 catalyst gives the highest amount of light olefins per gram of active Ru/HMOR used.

Table 4.2 Thermal conductivity of the studied Ru/HMOR-based catalysts

	Ru/HMOR[a]	**Kaolin[b]**	**α-alumina[b]**	**BC-20[c]**	**BC-30[c]**	**BC-40[c]**	**BC-50[c]**
Thermal conductivity (w/m.K)	0.16	14.9	3.12	10.8	9.30	7.8	6.4

[a] From Jakubinek *et al.*, 2007
[b] From Perry and Green (1997)
[c] Weighted-average

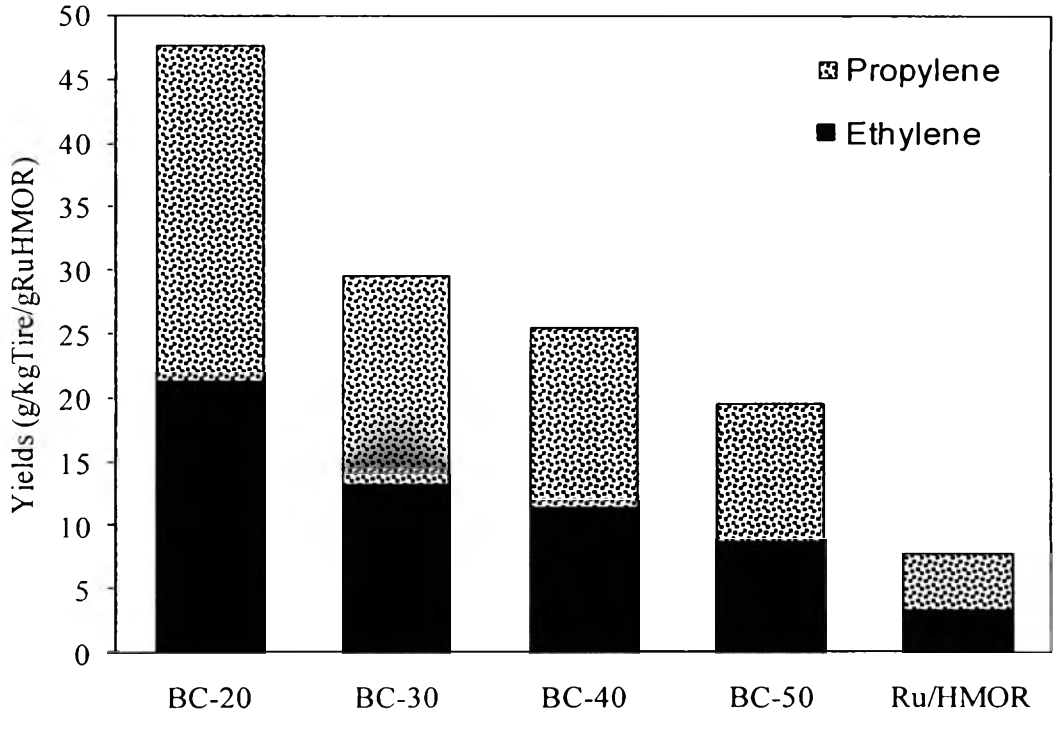

Figure 4.7 Light olefins production per kilogram of tire and gram of active Ru/HMOR.

4.1.5 Liquid Analysis

Liquid products obtained from the catalytic pyrolysis of waste tire were classified into 5 petroleum fractions by the boiling point and carbon range from SIMDIST-GC analysis as shown in Table 4.3.

4.1.5.1 Petroleum Fraction Analysis

According to Figure 4.8, the main fractions of maltene from the catalytic pyrolysis of waste tire are naphtha, kerosene, light gas oil, heavy gas oil, and residue. The amount of naphtha increases, and consequently that of kerosene, light gas oil, heavy gas oil, and residue decreases when all catalysts are used. It means that the Ru/HMOR-based catalysts can break down the chain of heavy molecules by cracking reactions. However, the naphtha is insignificantly changed upon the amount of active Ru/HMOR in the BC catalysts. Since no significance on the

weight percentage of naphtha was found, the naphtha yield per gram of tire and gram of active Ru/HMOR is compared as shown in Figure 4.9. It is found that the BC-20 catalyst gives the highest yield of naphtha per gram of active Ru/HMOR used. This is because the matrix, which help heat dissipation during the catalytic reaction and also can crack a large molecule which cannot diffuse to the zeolite pore.

Table 4.3 The boiling point and carbon ranges of refinery products (Nguyễn *et al.*, 2010)

Fraction	Carbon range	Boiling point (°C)
Naphtha	C_5-C_9	<200
Kerosene	C_{10}-C_{13}	200–250
Light gas oil	C_{14}-C_{20}	250–300
Heavy gas oil	C_{21}-C_{23}	300–370
Residue	C_{24}-C_{50}	>370

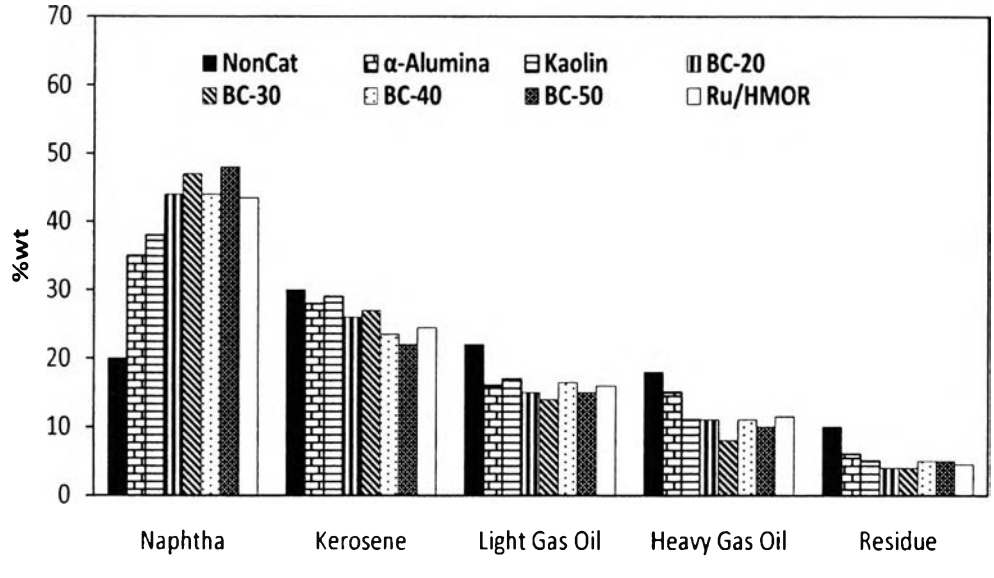

Figure 4.8 Petroleum Fractions in maltenes obtained from the catalytic pyrolysis of scrap tire using the Ru/HMOR-based catalysts with various compositions.

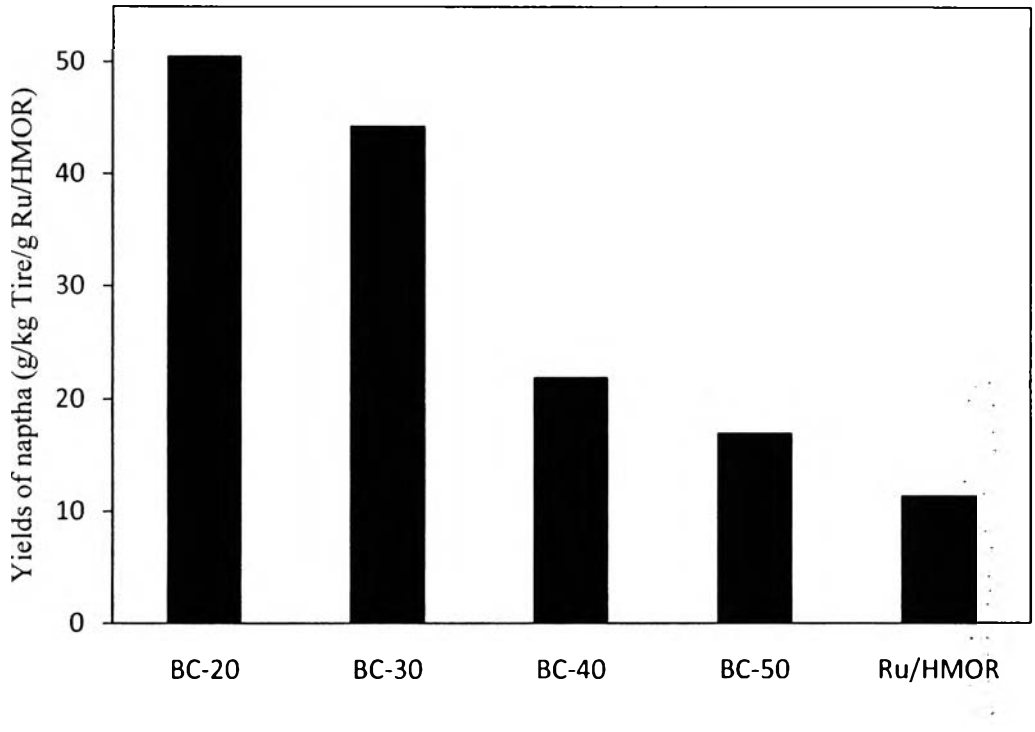

Figure 4.9 Naphtha production per kilogram of tire and gram of active Ru/HMOR.

4.1.5.2 Asphaltenes

The pyrolytic oils obtained from the catalytic pyrolysis of waste tire were mixed with n-pentane to precipitate asphaltene from the solution. Figure 4.10 shows the weight percentage of asphaltene in the pyrolytic oils obtained from different catalyst compositions. It can be observed that the amount of asphaltene is insignificantly different among the BC catalysts. However, the BC catalysts exhibit a higher potential for asphaltene reduction than the active Ru/HMOR zeolite. It might be because of the matrix in the studied catalyst. The matrix that surrounds the active Ru/HMOR zeolite leads to good heat dissipation during the cracking reaction, resulting in the increase in cracking of heavy hydrocarbon into light hydrocarbon molecules. Furthermore, Figure 4.10 indicates that kaolin itself can also reduce asphaltene in the oil; therefore, the matrix is capable of cracking large molecules, which cannot readily diffuse into zeolite pores. The resulting fragments are small enough to enter the zeolite pores.

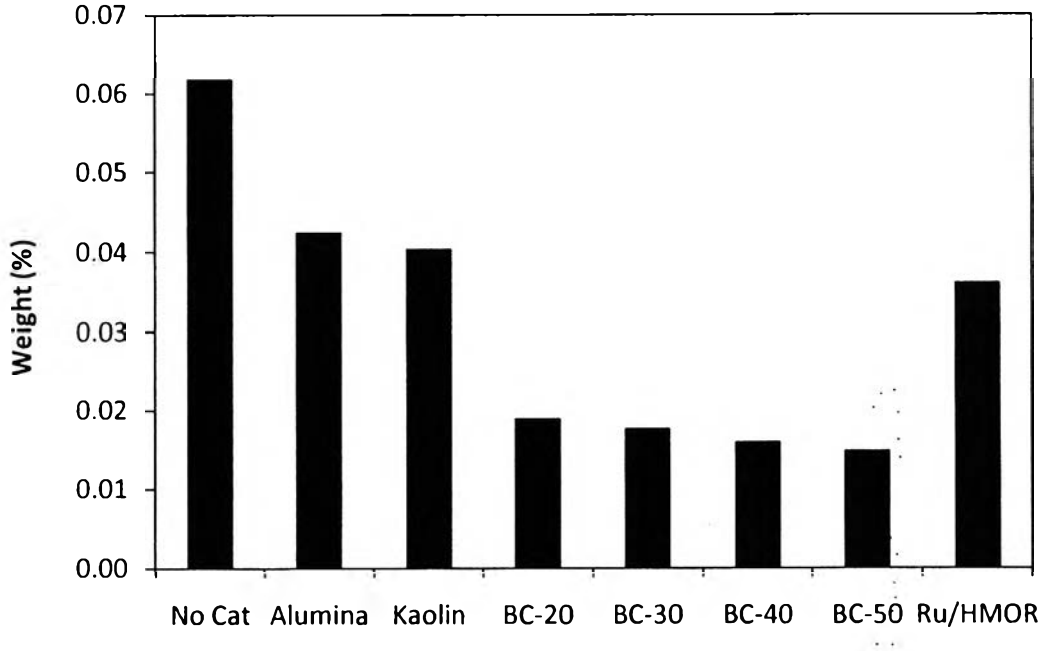

Figure 4.10 Weight percentage of asphaltene in pyrolytic oils obtained from the catalytic pyrolysis of scrap tire using the Ru/HMOR-based catalysts with various compositions.

The maltenes were separated into 5 fractions such as saturated hydrocarbons, mono-aromatics, di-aromatics, poly-aromatics, and polar-aromatics using liquid adsorption chromatography. Figure 4.11 demonstrates that the ratio of saturated hydrocarbons to total aromatic hydrocarbons and the ratio of mono-aromatics to total aromatic hydrocarbons increase with the increasing amount of active Ru/HMOR zeolite in the catalysts. However, all catalysts give a lower amount of saturated hydrocarbons when compared with the non-catalytic case because of the high hydrogenolysis activity of ruthenium clusters. On the other hand, mono-aromatic hydrocarbons from using the studied catalysts and the active Ru/HMOR zeolite can be produced in a higher amount than in the non-catalytic case. And, although the active Ru/HMOR zeolite content is increased in the studied catalysts, the amount of mono-aromatics is not significantly changed. It is also due to the effect of matrix, which acts as a heat transfer medium in the catalyst. During the catalytic reaction, the matrix helps heat dissipation, and prevents over-cracking.

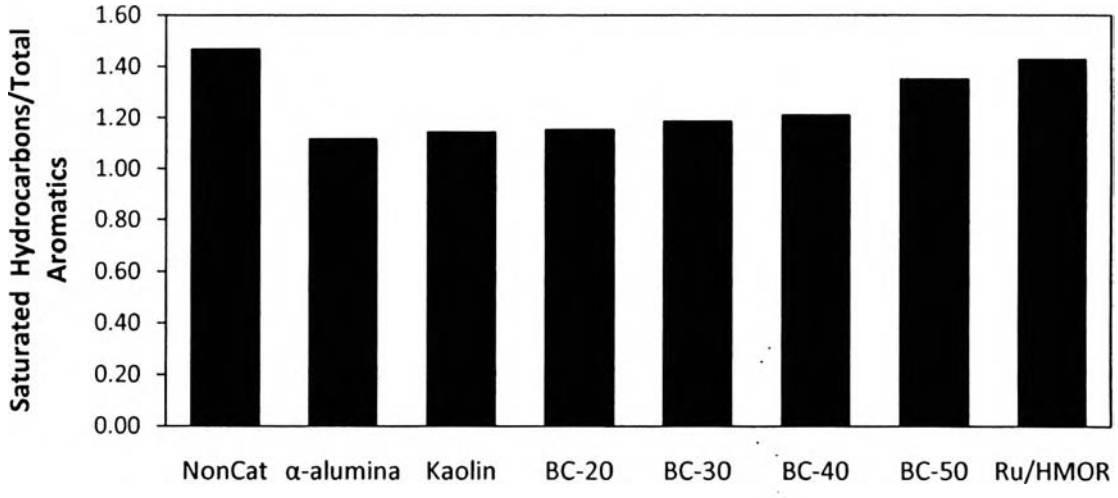

(a)

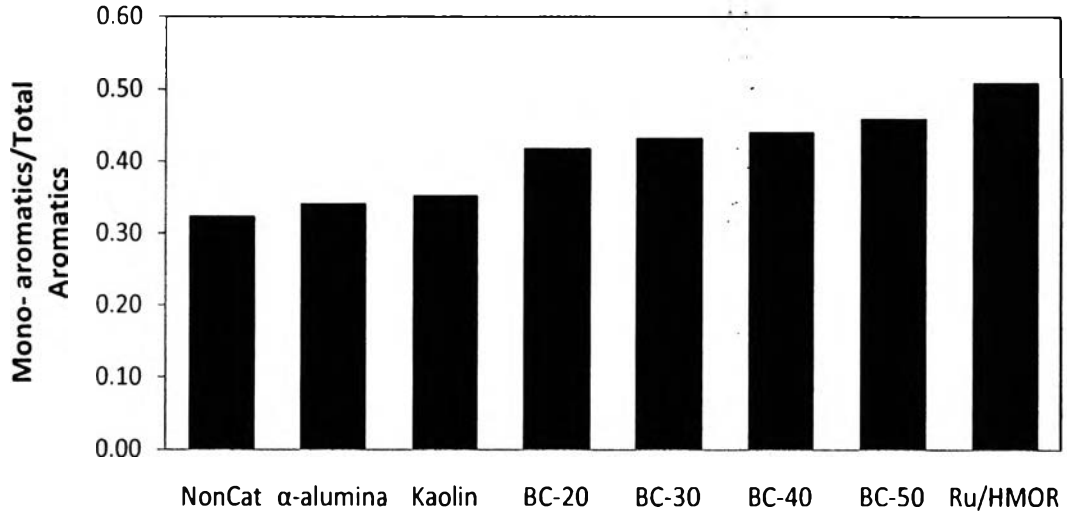

(b)

Figure 4.11 Chemical compositions in maltenes obtained from the catalytic pyrolysis of scrap tire using the Ru/HMOR-based catalysts with various compositions: (a) the ratio of saturated hydrocarbons to total aromatic hydrocarbons, and (b) the ratio of mono aromatic to total aromatic hydrocarbons.

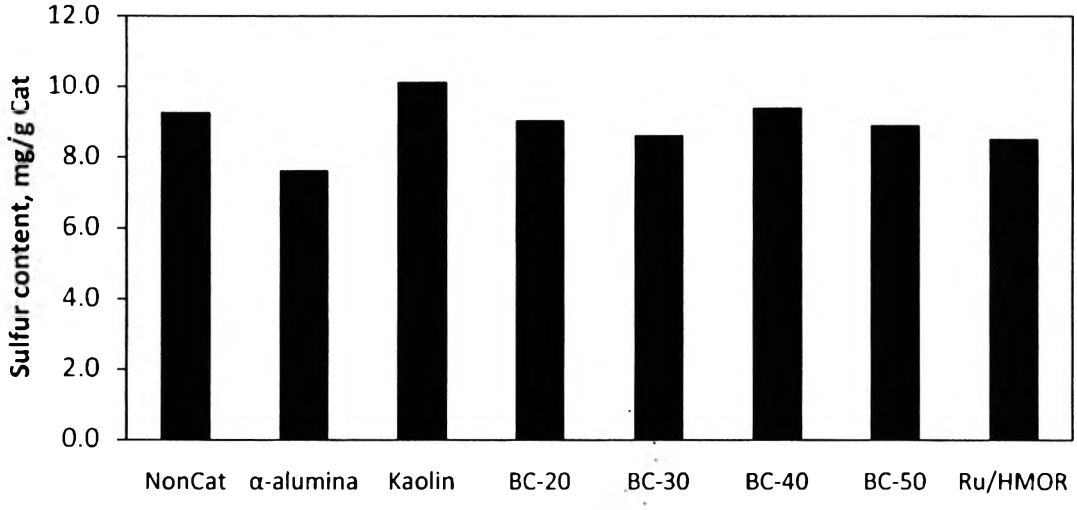

Figure 4.12 Sulfur content in pyrolytic oils obtained from the catalytic pyrolysis of scrap tire using the Ru/HMOR-based catalysts with various compositions.

Moreover, sulfur content in the pyrolytic product is important factor to qualify for the pyrolytic oil. The sulfur content in oil was measured by using elemental analyzer as shown in Figure 4.12. It can be seen that the sulfur content in the pyrolytic oils from using all catalysts is insignificantly different.

4.1.6 Spent Catalyst Characterization

The TG results showed two different weight loss positions. The first one observed at a low temperature of around 260°C, and the second one located around 410°C, which are divided to two different types of deposited hydrocarbons on the catalysts as shown in Figure 4.13. The active Ru/HMOR zeolite produces the higher amount of coke than the BC catalysts. In addition, among the studied catalysts, there is a trend of increasing coke formation with the increasing amount of the active Ru/HMOR zeolite. Namely, the amount of coke increases in the following order: BC-20 < BC-30 < BC-40 < BC-50.

The results of elemental analysis for sulfur contents in the spent catalysts are also displayed in Table 4.4. BC-20 exhibits the highest sulfur tolerance among Ru/HMOR-based catalysts as considered from its lowest sulfur content. Con-

sequently, the BC-20 exhibits the highest catalytic cracking activity (from Figure 4.7) with the least coke formation.

Table 4.4 Coke and sulfur in the spent catalysts

Catalyst	Coke (g/g cat.)	Sulfur (mg/g cat.)
Ru/HMOR	0.38	5.32
Kaolin	0.30	4.96
α-alumina	0.074	1.44
BC-20	0.27	5.11
BC-30	0.30	5.85
BC-40	0.35	5.96
BC-50	0.35	6.83

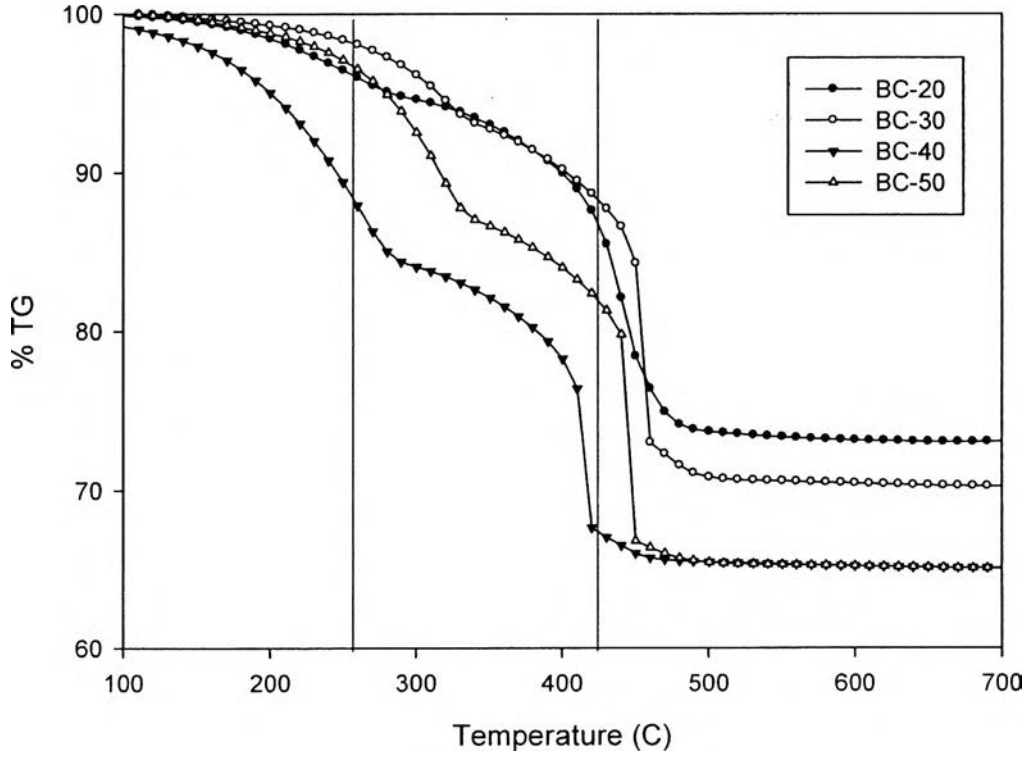

Figure 4.13 The TG results of the studied Ru/HMOR-based catalysts.

From all of above-mentioned results, the Ru/HMOR-based catalysts exhibit a higher potential for desirable productions (light olefins) than the pure Ru/HMOR because of a matrix function. Since the major function of the matrix is to support the zeolite particles and also to form a diffusion medium for the hydrocarbon molecules. Another function is to behave as a diluent media for the zeolite activity moderate and as a heat carrier helping heat transfer or heat dissipate during cracking reaction (Bhatia, 1946).

Cracking reaction is a breaking of the long hydrocarbon chains into shorter hydrocarbon molecules. There are two parallel mechanisms. One is a thermal cracking, and another is a catalytic cracking. The catalytic cracking reaction is mainly occurred through the intermediate of a carbenium ion. The first step begins with the reaction of a hydrocarbon molecule at the acidic sites of the catalyst to form a carbenium ion. Then, the carbenium ions are isomerization, beta-scission, and hydrogen transfer (Yang, 2003).

The heat dissipation has a critical role in the cracking reaction. It can prevent the over-cracking, which occurs from hotspots on a catalyst. Moreover, a carbenium ion can be easily formed from olefins by thermal effect on catalyst-oil contact. Therefore, the Ru/HMOR-based catalysts, which consist of a matrix, can dissipate heat during the cracking reaction, leading to a high yield of light olefins as compared to the pure Ru/HMOR zeolite. The Ru/HMOR zeolite does not have the matrix. This, of course, leads to poor heat distribution during the cracking reaction, then hotspot, and finally over-cracking.

In conclusion, the BC-20 exhibits the highest light olefins and naphtha productions with the least coke formation and the highest sulfur tolerance. Since the active component (Ru/HMOR) of the catalyst is often expensive. Therefore, it is more economic to use the BC-20. It can be concluded that the best composition of the Ru/HMOR-based catalyst for light olefins production from waste tire pyrolysis is 20%wt of Ru/HMOR, 70%wt of Kaolin, and 10%wt of α-alumina, which is the BC-20 catalyst.

4.2 Effect of Ratio of D_{pellet} to $D_{reactor}$

The actual size and shape of the fabricated catalyst is influenced by mass transfer and reactor pressure drop. As the catalyst pellet size is increased, the pressure drop through the reactor decreases. However, as the size of catalyst pellet is increased there comes a point where the catalyst activity is limited by diffusion within the catalyst. Therefore, the effect of the catalyst pellet size is investigated. The catalyst, which consists of Ru/HMOR 20 %wt, kaolin 70 %wt, and α-alumina 10%wt (BC-20) was prepared by extrusion for different pellet diameters (1.0, 2.0, 3.0, and 4.0 mm). The influence of ratio of pellet diameter to reactor diameter ($D_{pellet}/D_{reactor}$) is summarized as follows.

The properties of the studied catalysts have been summarized in Table 4.5. The data include the pore volume and surface area in the fresh catalysts, and the amount of sulfur and coke in the spent catalysts.

Table 4.5 Physical properties of the fresh catalysts and the coke and sulfur contents in the spent catalysts

Catalyst diameter (mm)	d/D*	Pore volume (cm^3/g)	Surface area (m^2/g)	Coke (g/g cat.)	Sulfur (mg/g cat.)
1.0	0.0185	0.20	120.2	0.26	5.85
2.0	0.0370	0.29	112.7	0.27	5.11
3.0	0.0556	0.95	108.1	0.29	2.18
4.0	0.0740	0.98	97.29	0.28	3.90

* d—pellet diameter and D—reactor diameter = 54 mm

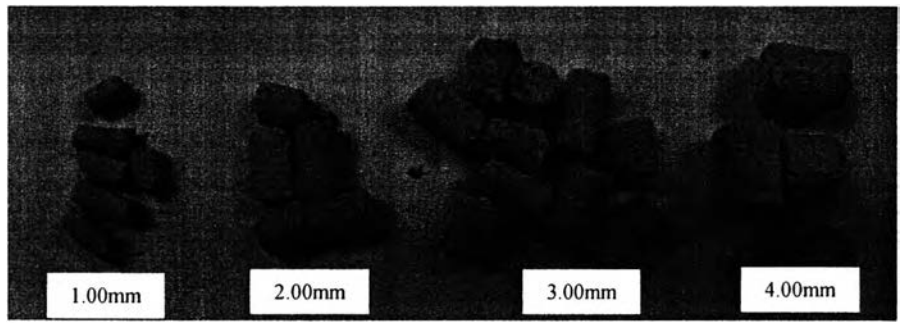

Figure 4.14 An appearance of the studied Ru/HMOR-based catalysts with various pellet diameters.

4.2.1 Pyrolysis products

Figure 4.15 shows the ratio of gas to liquid obtained from using the catalysts with various the ratios of pellet diameter to reactor diameter. It is found that the ratio of gas to liquid slightly increases with the increasing ratio of pellet diameter to reactor diameter from 0.0185 to 0.0740.

In the experiment, the solid yields for both catalytic and non-catalytic cases remain constant at about 45 %wt by average because the tire is completely cracked.

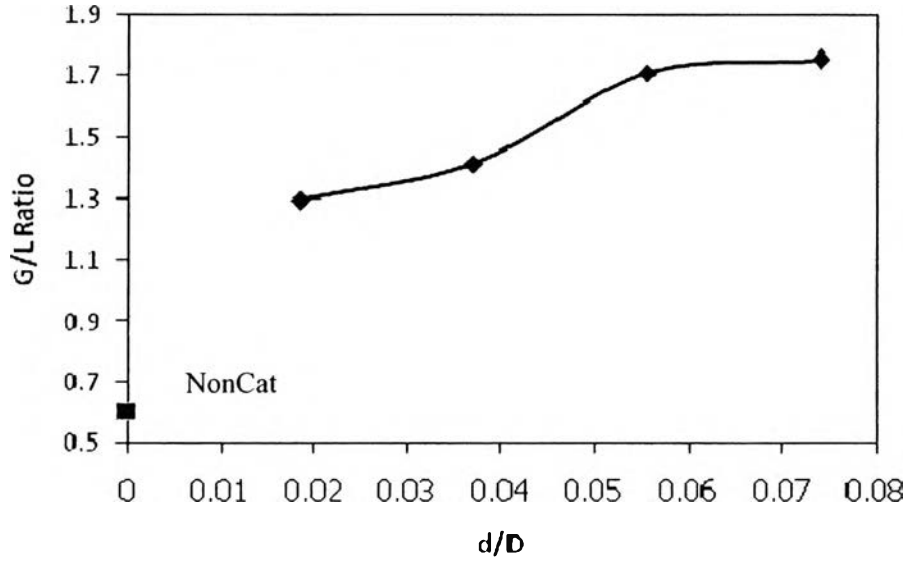

Figure 4.15 Gas to liquid ratio obtained from the catalytic pyrolysis of scrap tire using the BC-20 catalyst with various ratios of pellet diameter to reactor diameter.

Light olefins production is the purpose of this research. The variation of light olefins yield with various ratios of pellet diameters to reactor diameters of the BC-20 catalyst is displayed in Figure 4.16. The yield of light olefins passes through the maximum at the ratio of 0.0556, and then remains constant as the ratio increases to 0.0740. It might be due to external and internal mass transfer through the pellets of the catalysts. The accessibility of the reactants to the catalytic surface, and the significant influence of external mass transfer such as at a low fluid flow rate occur from the increasing diffusion length of reactant from bulk solution to the catalyst surface. On the other hand, with the increase of catalyst film thickness or the size of catalyst, the internal mass transfer may play a dominant role by limiting the application of the catalyst near the support–catalyst interface.

In addition, the liquid products were classified to 5 fractions in terms of petroleum fractions as presented in Figure 4.17. Naphtha fraction is slightly increased with increasing the ratio from 0.0185 to 0.0556, but slightly decreases when the ratio reaches 0.0740. Consequently, kerosene, light gas oil, heavy gas oil, and residue decrease. And, the ratio of 0.0556 gives the highest naphtha fraction.

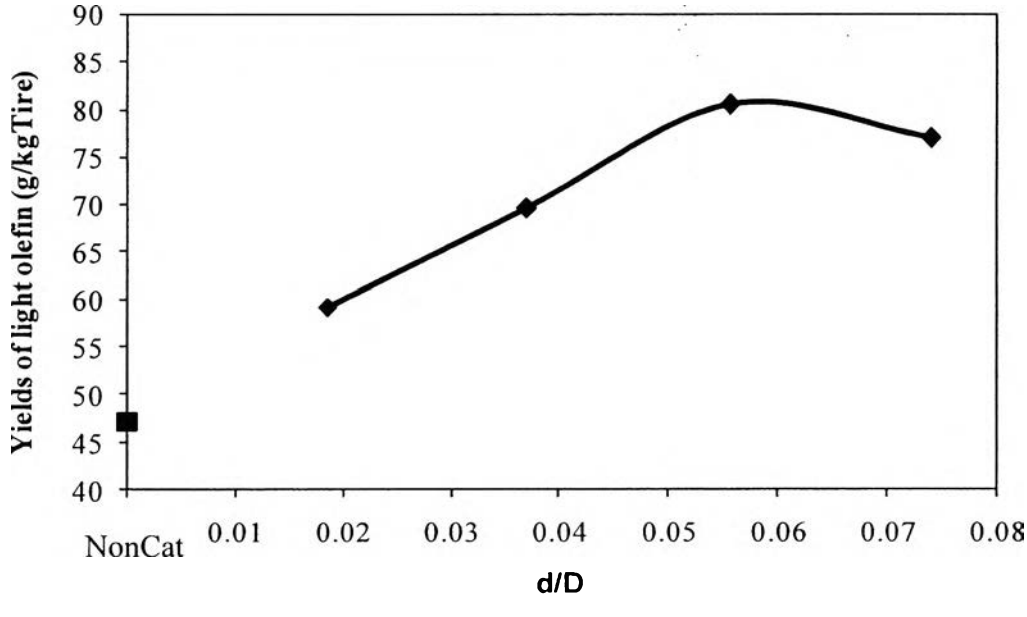

Figure 4.16 Light olefins production obtained from the catalytic pyrolysis of scrap tire using the BC-20 catalyst with various ratios of pellet diameter to reactor diameter.

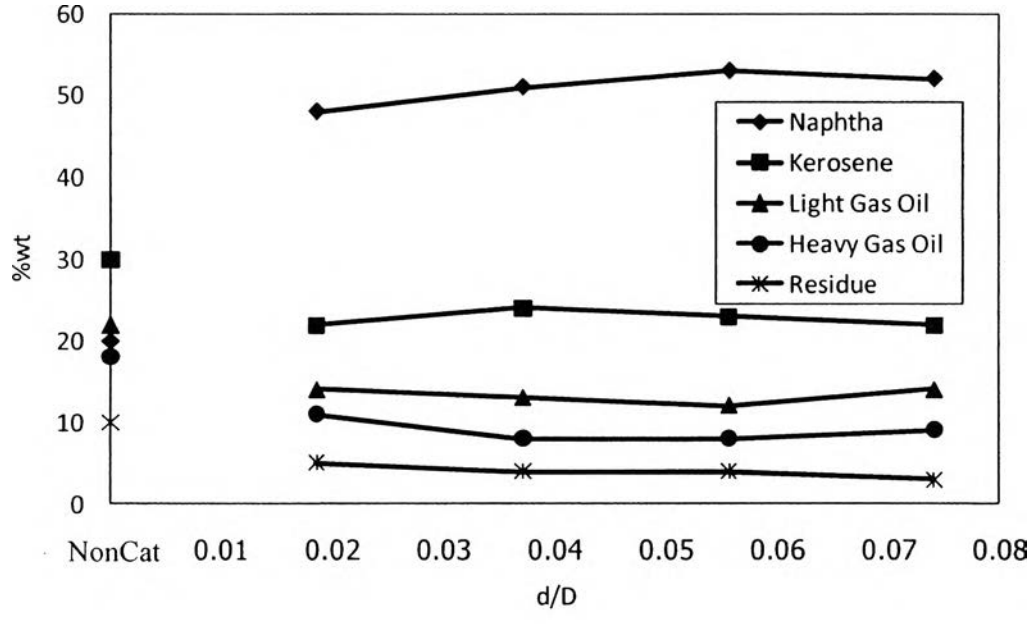

(a)

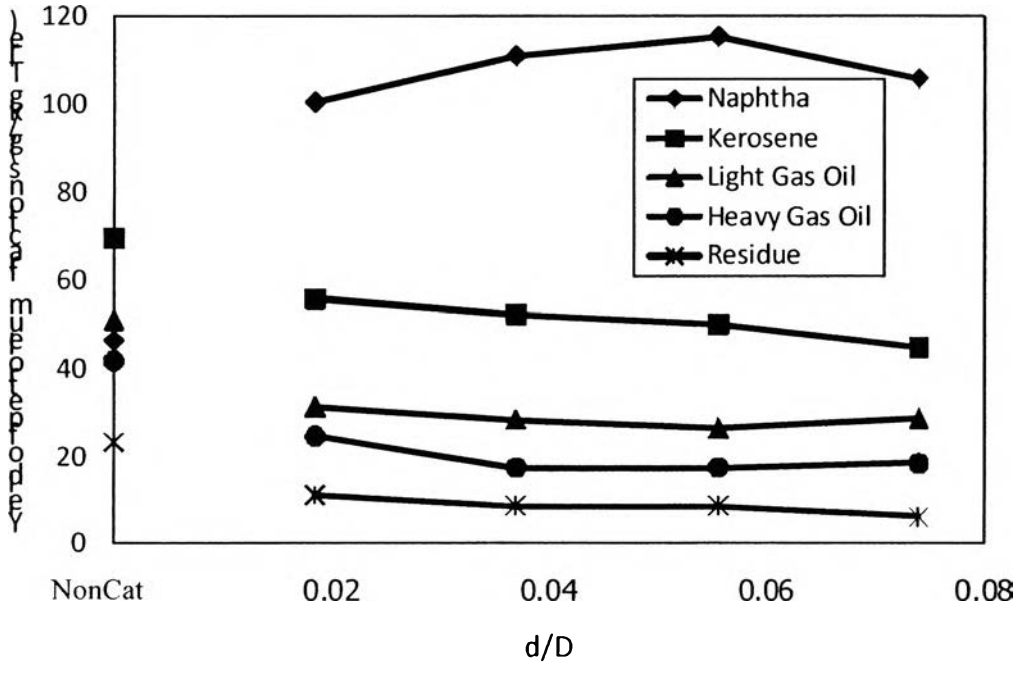

(b)

Figure 4.17 Petroleum Fractions in maltenes obtained from the catalytic pyrolysis of scrap tire using the BC-20 catalyst with various ratios of pellet diameter to reactor diameter: (a) weight percentage, and (b) yield per kg. of tire.

4.2.2 Quality of Pyrolysis Products

Figure 4.18 shows the weight percentage of asphaltene in the pyrolytic oils with various ratios of pellet diameter to reactor diameter. It can be observed that the amount of asphaltene decreases with the increasing ratio of pellet diameter to reactor diameter from 0.0185 to 0.0556. Moreover, the ratio of 0.0556 exhibits the minimum amount of asphaltene in the experiments.

However, the chemical composition in the oil products was separated into 5 functional groups such as saturated hydrocarbons, mono-, di-, poly-, and polar-aromatics. The ratio of saturated hydrocarbons to total aromatics is displayed in Figure 4.19. It can be seen that the ratio slightly decreases with the increasing the ratio of pellet diameter to reactor diameter from 0.0185 to 0.0740. Furthermore, the ratio of mono-aromatic to total aromatics is shown in Figure 4.20. It is found that the ratio of pellet diameter to reactor diameter of 0.0556 exhibits the highest ratio of mono-aromatic to total aromatics.

In addition, the sulfur content in oil was measured by using elemental analyzer as shown in Figure 4.21. It can be seen that the sulfur content in the pyrolytic oil from using the BC-20 catalyst at the ratio of 0.0370 is the highest.

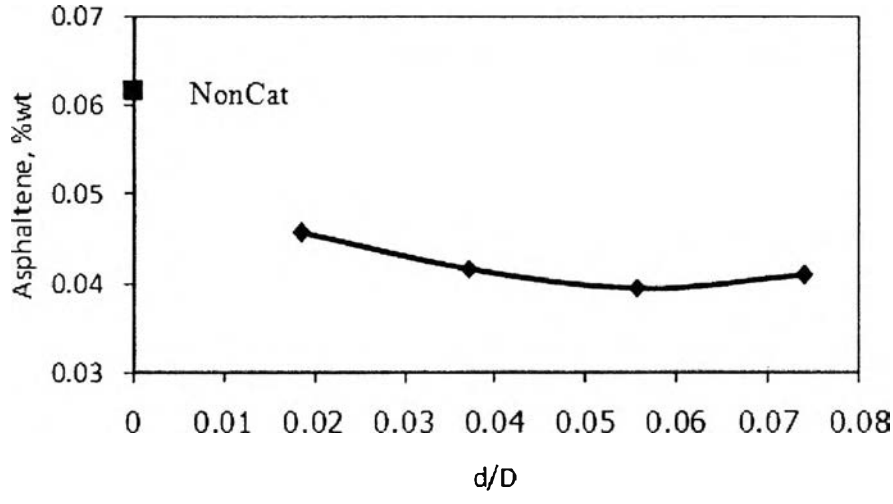

Figure 4.18 Weight percentage of asphaltene in the pyrolytic oils obtained from the catalytic pyrolysis of scrap tire using the BC-20 catalyst with various ratios of pellet diameters to reactor diameters.

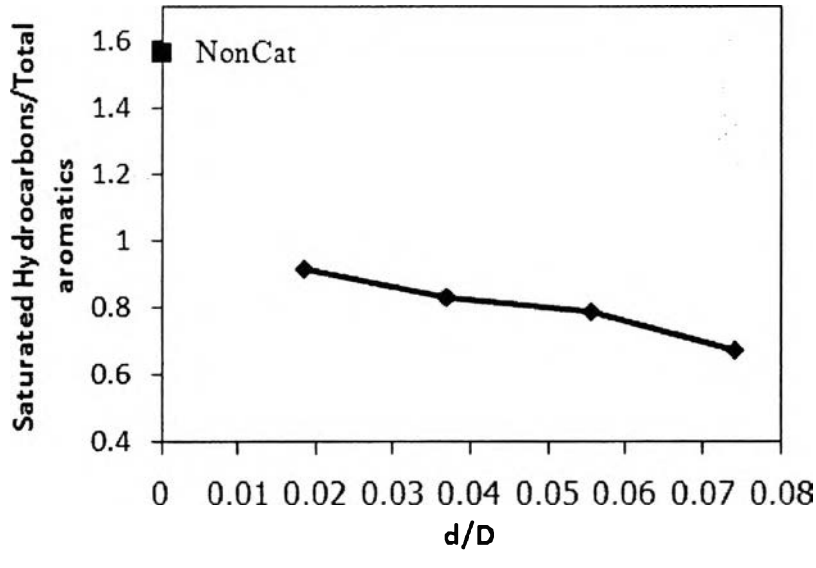

Figure 4.19 The ratio of saturated hydrocarbons to total aromatics in the maltenes obtained from the catalytic pyrolysis of scrap tire using the BC-20 catalyst with various ratios of pellet diameter to reactor diameter.

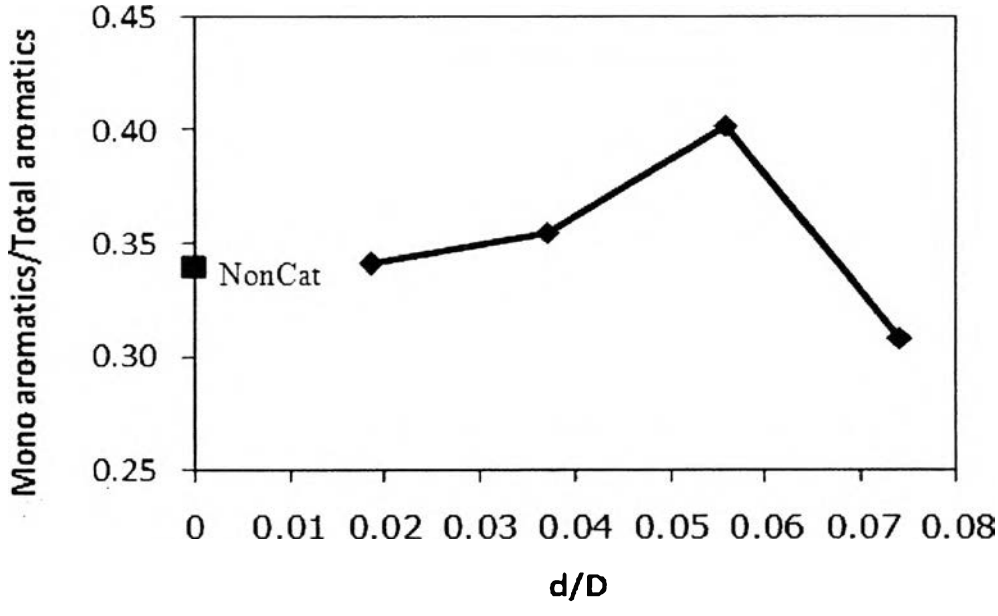

Figure 4.20 The ratio of mono-aromatic to total aromatics in the maltenes obtained from the catalytic pyrolysis of scrap tire using the BC-20 catalyst with various ratios of pellet diameter to reactor diameter.

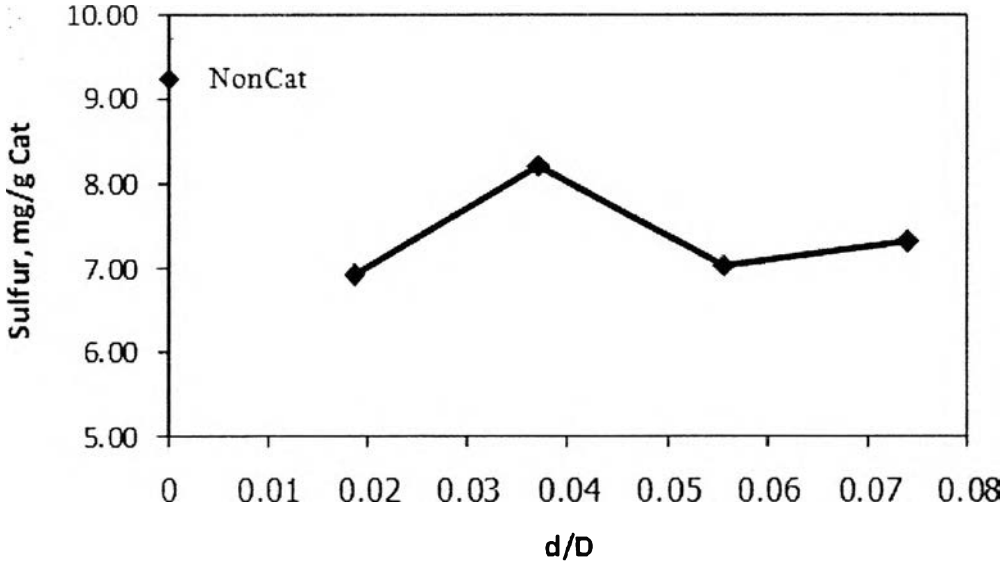

Figure 4.21 Sulfur in the pyrolytic oils obtained from the catalytic pyrolysis of scrap tire using the BC-20 catalyst with various ratios of pellet diameter to reactor diameter.

From all of above-mentioned results, the ratio of pellet diameter to reactor diameter of 0.0556 (the pellet diameter of 3.0 mm) exhibits a high light olefins production in the gaseous product, and naphtha fraction and mono-aromatics in the oil product. And, consequently low asphaltene and sulfur content were acheived. So, the ratio of pellet diameter to reactor diameter of 0.0556 is the most appropriate size for this reactor (the bench-scale autoclave reactor). It might be because of transport limitations on the solid-catalyst reaction.

Figure 4.22 describes the reactant concentration profile of the surrounding of a catalyst particle. There are two regions. In Region 1, the reactant diffuses through the stagnant boundary layer that surrounds the particle. The transport phenomena in this region occur outside the catalyst particle, which they are commonly referred to as external transport effect. In Region 2, the reactant diffuses into the pores of the catalyst particle, and transport phenomena in this region are called internal transport effects. Both external and internal transport effects can be important in a catalytic reaction (Davis *et al.*, 2003).

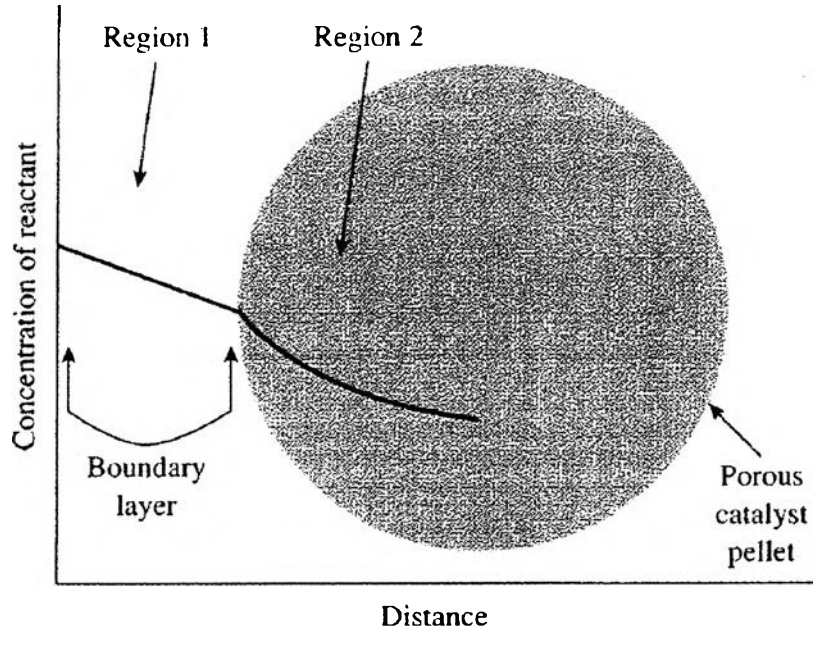

Figure 4.22 Concentration profile of a reacting species in the vicinity of a porous catalyst particle (Davis *et al.*, 2003).

This work involves the internal transport effect since it was the study of the influence of the pellet diameter. The *Thiele modulus*, ϕ, and the *effectiveness factor*, η, are defined as shown in Eq. (3) (Davis *et al.*, 2003):

$$\eta \equiv \frac{rate\ of\ reaction\ with\ pore\ diffusion\ resistance}{rate\ of\ reaction\ with\ surface\ conditions},$$

$$\phi \equiv \sqrt{\frac{instrinsic\ rate}{diffusion\ coefficient}} \tag{3}$$

For a reaction with an n^{th} order reaction rate, the Thiele modulus can be calculated using Eq. (4) with L_P the length parameter, k the intrinsic reaction rate constant, D_{TA}^{e} the effective transition diffusivity, and C the reactant concentration inside the particle, which is lower than the bulk concentration, if diffusion limitation occurs. The effectiveness factor is given by Eq. (5) (Davis *et al.*, 2003):

$$\phi = L_P \sqrt{\frac{kC^{n-1}}{D_{TA}^{e}}} \tag{4}$$

$$\eta = \frac{\tanh(\phi)}{\phi} \tag{5}$$

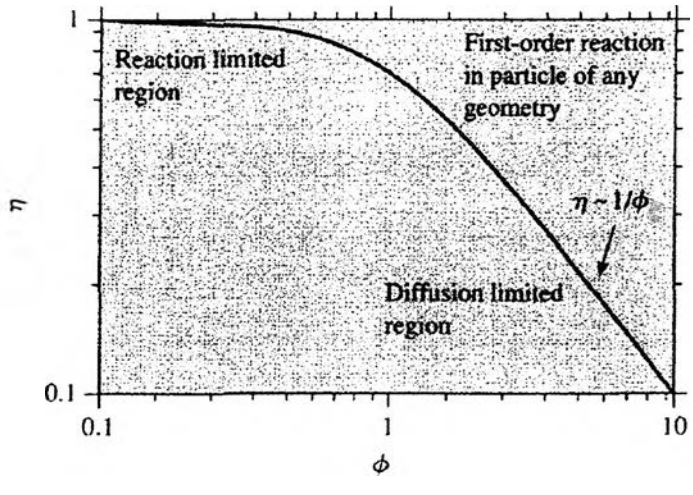

Figure 4.23 Effectiveness factor $[\eta = \frac{\tanh(\phi)}{\phi}]$ for a first-order reaction in a catalyst as a function of the Thiele modulus with generalized length parameter (Davis *et al.*, 2003).

The length parameter is defined by Eq. (6) with the pellet volume, V_P, the external surface area, S_P (Davis *et al.*, 2003).

$$L_P = \frac{V_P}{S_P} \tag{6}$$

Thus, the length parameter for the cylinder (Figure 4.24) is given by Eq. (7) with the radius of a catalyst particle, R_P.

$$L_P = \frac{R_P}{2} \tag{7}$$

And the Thiele modulus is defined by Eq. (8)

$$\phi = \frac{R_P}{2}\sqrt{\frac{kC^{n-1}}{D_{TA}^e}} \tag{8}$$

For the effective transition diffusivity, D_{TA}^e is calculated from the Bosanquet equation (Eq. (9)) with the effective Knudsen diffusivity, D_{KA}^e and the effectiveness molecular diffusivity, D_{AB}^e.

$$\frac{1}{D_{TA}^e} = \frac{1}{D_{AB}^e} + \frac{1}{D_{KA}^e} \tag{9}$$

The Knudsen diffusivity is calculated from Eq. (10).

$$D_{KA} = (9.7 \times 10^3) \cdot R_{pore} \cdot \left(\frac{T}{M_A}\right)^{1/2} \tag{10}$$

where R_{pore} is the pore radius in cm, T is the absolute temperature in Kelvins, and M_A is the molecular weight of A.

And the superscript *e* refer to the *effective* diffusivity, which can be calculated from Eq. (11) with the porosity of the pellet, ε_P, is defined as the ratio of void volume within the pellet to the total pellet volume (void + solid) and the tortuosity, τ, is the ratio of the zig-zag length to the straight length.

$$D^e = \frac{\varepsilon_P}{\tau} D \tag{11}$$

The criteria for importance of diffusional limitations (Froment and Bischoff, 1990):

1. For $\phi << 1$, $\eta = 1$ (no diffusion limitation)
2. For $\phi >> 1$, $\eta = 1/\phi$ (diffusion limitation)

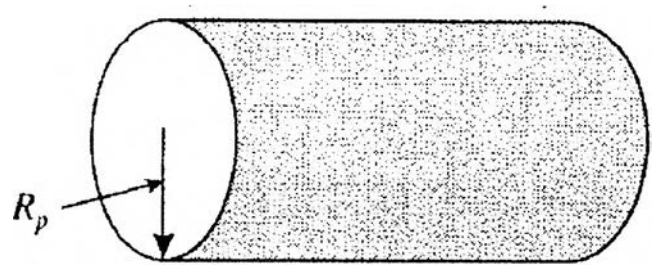

Figure 4.24 Scheme of a cylindrical catalyst particle (Davis *et al.*, 2003).

Cracking reaction consists of many reactions such as hydrogenation, dehydrogenation, cracking, isomerization, and alkylation. Dehydrogenation reaction is presented as an example (Eq. (12)).

$$\text{Alkane} \xrightarrow[-H_2]{Ru} \text{Alkene},$$

$$\text{n-hexane} \xrightarrow[-H_2]{Ru} \text{n-hexene} \qquad (12)$$

The effectiveness factor of 1 means the rate of reaction with the surface condition or no diffusion limitation. The rate constant of reaction can therefore be determined at the maximum effectiveness factor of 1 and the Ru/HMOR diameter of 0.042 cm (40 meshes within non-diffusion limitation region).

Given: R_P = 0.021 cm

D_{AB} n-hexane (Perry and Green (1997)) = 0.0757 cm^2/s

ε_P (from the experimental data) = 0.63

τ (network of randomly oriented cylindrical pores = 3(Davis *et al.*, 2003)

R_{pore} (from the experimental data) = $34.64*10^{-8}$ cm

T (from the experimental data) = 300°C = 573 K

The effective Knudsen diffusivity is:

$$D_{KA} = (9.7 \times 10^3) \cdot (34.64 \times 10^{-8} cm) \cdot \left(\frac{573K}{86}\right)^{\frac{1}{2}} = 0.00868\ cm^2 \cdot s^{-1}$$

$$D_{KA}^e = \frac{0.63}{3} \cdot 0.00868 = 0.00182\ cm^2 \cdot s^{-1}$$

The effectiveness molecular diffusivity is:

$$D_{AB}^{e} = \frac{0.63}{3} \cdot 0.0757 = 0.0159\ cm^2 \cdot s^{-1}$$

The effective transition diffusivity is:

$$\frac{1}{D_{TA}^{e}} = \frac{1}{0.0159} + \frac{1}{0.00182}$$

$$D_{TA}^{e} = 0.001633\ cm^2 \cdot s^{-1}$$

The Thiele modulus for the first-order is:

$$\phi = \frac{0.021}{2}\sqrt{\frac{k}{0.001633}} = 0.26\sqrt{k}$$

Recall that the effectiveness factor can be approximated by:

$$\eta = \frac{\tanh(\phi)}{\phi} = 1.0$$

From Figure 4.22 $\phi = 0.1$

$$0.1 = 0.26\sqrt{k}$$

$$k = 0.148\ s^{-1}$$

So, the rate constant of this reaction with no diffusion limitation is $0.148s^{-1}$. The effectiveness factor of each pellet diameter at this reaction rate constant can subsequently be calculated and shown in Table 4.6.

From the result, the most oppropriate pellet size of 3.0 mm that can be used in the bench-scale autoclave reactor.

Table 4.6 The effectiveness factors of each pellet diameter

Catalyst diameter (mm)	R_P **(cm)**	ϕ	η
1.0	0.05	2.90	0.42
2.0	0.10	1.50	0.63
3.0	0.15	1.30	0.68
4.0	0.20	1.46	0.65

However, the appropriate ratio of pellet diameter to reactor diameter is based on reactor size and reactor type. Moreover, the extrusion is a significant factor in terms of porosity. It influences the effective diffusivity.

In conclusion, the pellet diameter of 3.0 mm. exhibits the highest catalytic cracking activity with the maximum asphaltene reduction. It can be concluded that the best ratio of pellet to reactor diameter is 0.0556 for the bench-scale autoclave reactor.

4.3 Deactivation of catalyst by coking

One of the major problems related to the heterogeneous catalysis operation is the catalyst loss of activity with time on stream, i.e. deactivation. Deactivation is generally divided into four classes; namely poisoning, coking or fouling, sintering and phase transformation. In this research, the deactivation by coking is emphasized. The deactivation of catalysts by coke formation was studied for 1 to 3 cycles of operation. The results and discussions are presented as follows. The spent catalysts were regenerated at 650°C for 30 minutes before the next operation. In order to reach the longest life from the catalyst, the catalyst must be regenerated in order to remove coke. Furthermore, the regeneration restores the catalyst to its full potential and spares the operator from repeatedly buying new catalyst.

4.3.1 Catalyst characterization

The XRD patterns of the fresh catalyst and regenerated catalysts are shown in Figure 4.25. These patterns indicate that the regeneration of catalyst did not affect the structure of the catalysts.

Table 4.6 summarizes the physical and chemical properties of the regenerated catalysts. The surface area, pore volume, and pore size of the catalysts were measured by using the BET method. And, the surface area and pore volume of the regenerated catalysts are slightly decreased with the increasing number of cycles.

The pore size distribution is shown in Figure 4.26. The average pore size diameter of the regenerated catalysts is slightly decreased, possibly caused by the blockage of a large pore by coke, leading to the decrement of the pore size di-

ameter. The partially covered pores then became a high amount of smaller pores. The pore blockage might be the reason for the reduction in pore volume also. In addition, the coke deposition on the regenerated catalysts obtained from TG experiment is shown in Table 4.7. The coke deposition slightly increases with increasing the number of cycles. The sulfur deposition on the regenerated catalysts is analyzed by an elemental analyzer. The results are shown in Table 4.8. When the number of cycles increases, the sulfur deposition on the regenerated catalysts also increases.

Moreover, the metal particle size and dispersion were determined by H_2-chemisorption, as displayed in Table 4.7. The metal particle size increases with the number of cycles. It might be because of the agglomeration of metal during catalyst regeneration by the heat generated from coke combustion (Scherzer and Gruia, 1996). Therefore, the catalysts after coke removal show a significant loss in hydrogenation and/or dehydrogenation activity due to noble metal agglomeration.

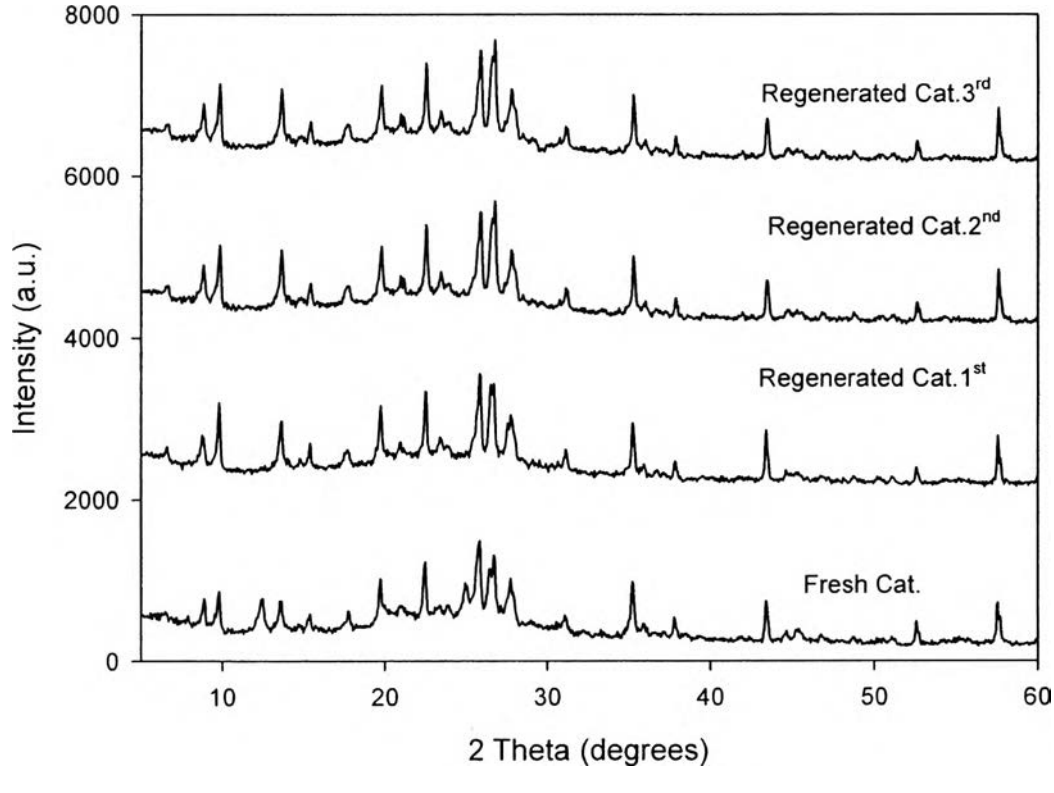

Figure 4.25 The XRD patterns of the catalysts.

Table 4.7 Physical properties of the regenerated catalysts

No. of cycles	Pore volume (cm^3/g)	Surface area (m^2/g)	Coke (g/g.cat)	Sulfur (mg/g. cat)	Dispersion (%)[a]	Ru particle size (nm)[a]
1	0.98	108.05	0.000	0.00	66.67	1.93
2	0.70	105.50	0.018	0.0296	64.33	2.00
3	0.61	105.08	0.020	0.0369	62.14	2.07

[a] Determined by H_2 chemisorptions

Table 4.8 Coke and sulfur contents in the spent catalysts

No. of cycles	Coke (g/g.cat)	Sulfur (mg/g. cat)
1	0.27	2.18
2	0.293	6.58
3	0.30	7.43

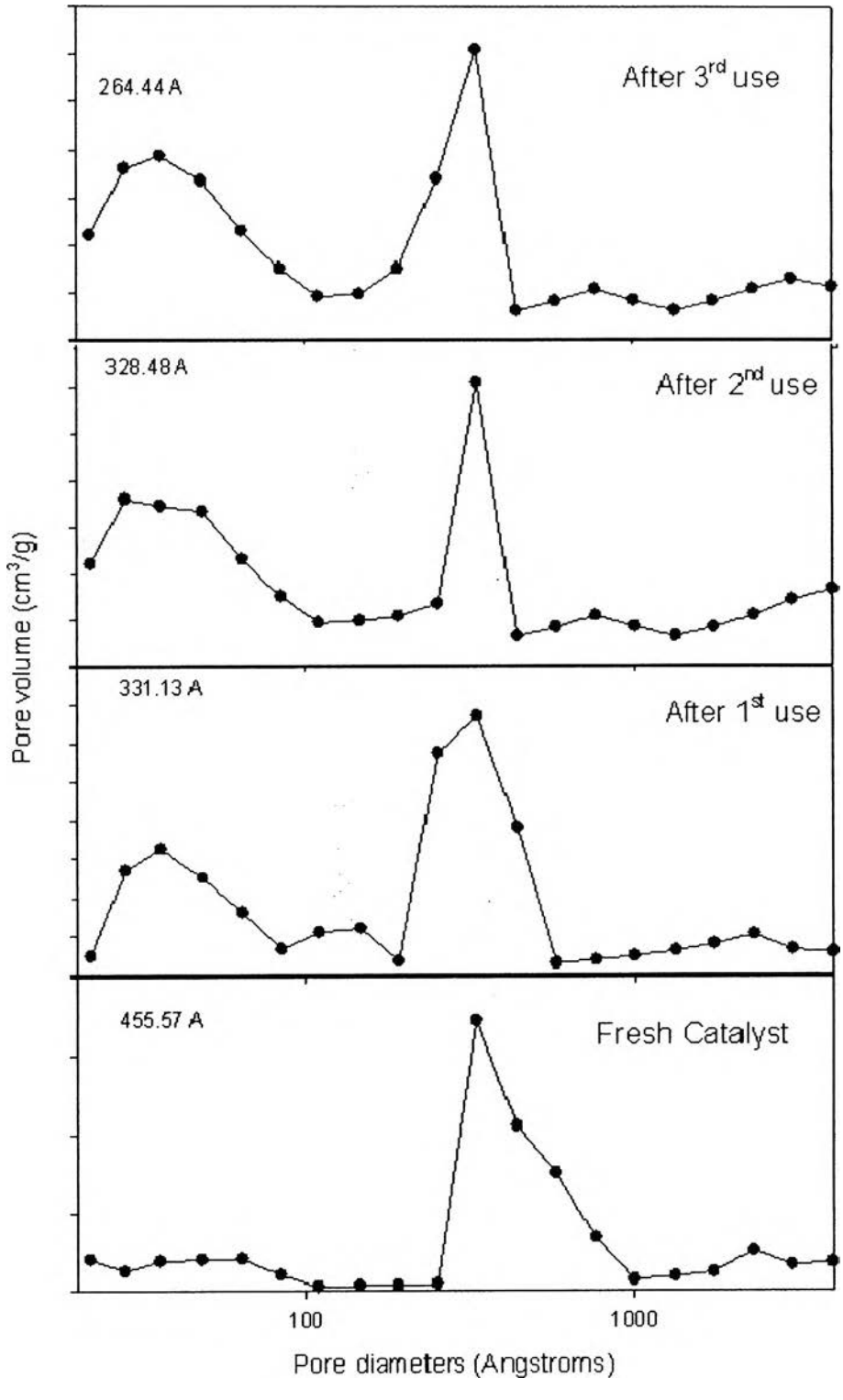

Figure 4.26 Variation of the pore sizes of the regenerated catalysts.

Conclusively, the coke formation on the catalysts increased with increasing the number of cycles. In general, the spent catalysts being charged to the regeneration may contain about 2 wt% to about 15 wt% cokes, and the regenerated catalysts from the regenerator contain less than 2 wt% coke (Cetinkaya *et al.*, 2005). The regenerated catalysts from 1 to 3 cycles in this work contain coke less than 2 wt%. Moreover, coke deposition could be predicted by the extrapolation of the plot between No. of cycles and coke content as shown in Figure 4.27.

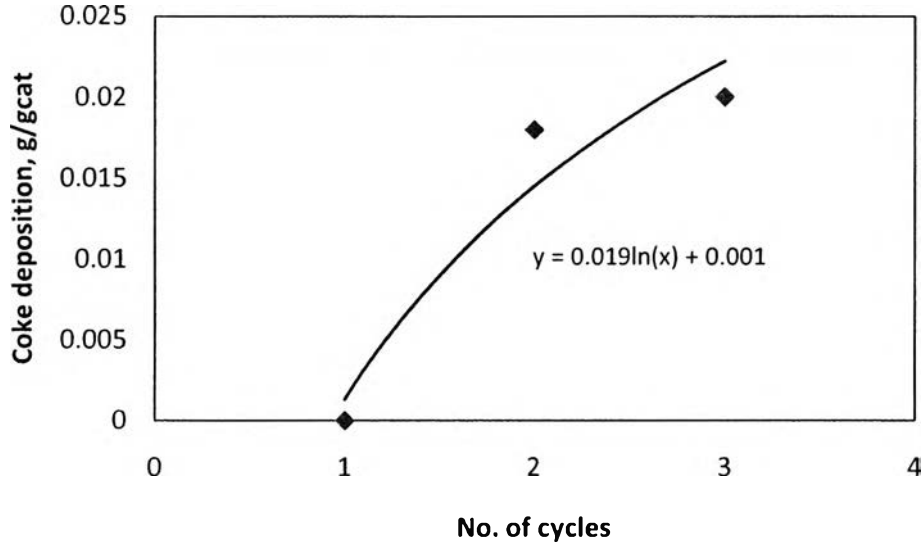

Figure 4.27 Relationship between the wt% coke deposition and the number of cycle.

4.3.2 Pyrolysis products

Figure 4.28 shows the change in the gas to liquid ratio with the number of cycles of catalyst reuse with the same conditions. One can see that the gas to liquid ratio decreases with the increasing number of cycles of catalyst reuse. The gas product at the 2nd cycle and the 3rd cycle of operation decreases about 2% and 6% as compared to the 1st cycle, respectively. It can be due to the coke deposition, which occurs in the pores and on the surface of the catalysts, and always leads to the loss of activity and product selectivity (Tailleur, 2008).

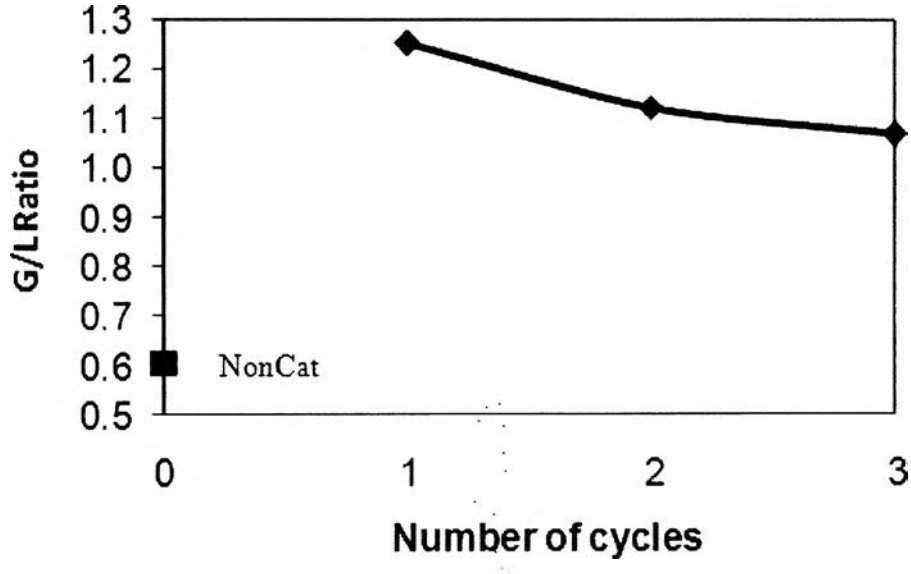

Figure 4.28 Gas to liquid ratio obtained from 1 to 3 cycles of operations.

Figure 4.29 exhibits the yield of gas composition with the number of cycles of catalyst reuse. It can be seen that the light gases decrease with the increasing numbers of cycles of catalyst reuse. Ethylene and propylene also decrease with the increasing numbers of cycles of catalyst reuse. Therefore, the light olefins production slightly reduces as presented in Figure 4.30. It means that the increase in the numbers of cycles of catalyst reuse leads to the reduction in the cracking activity of the catalysts. The lessening in the cracking activity of the catalysts is caused mainly by coke deposition and metal agglomeration.

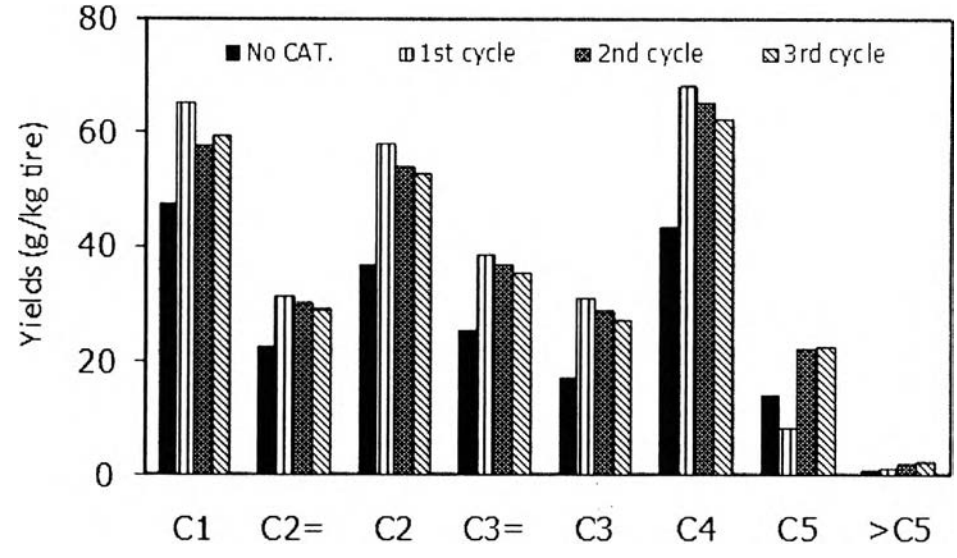

Figure 4.29 Yields of gas compositions obtained from 1 to 3 cycles of operations.

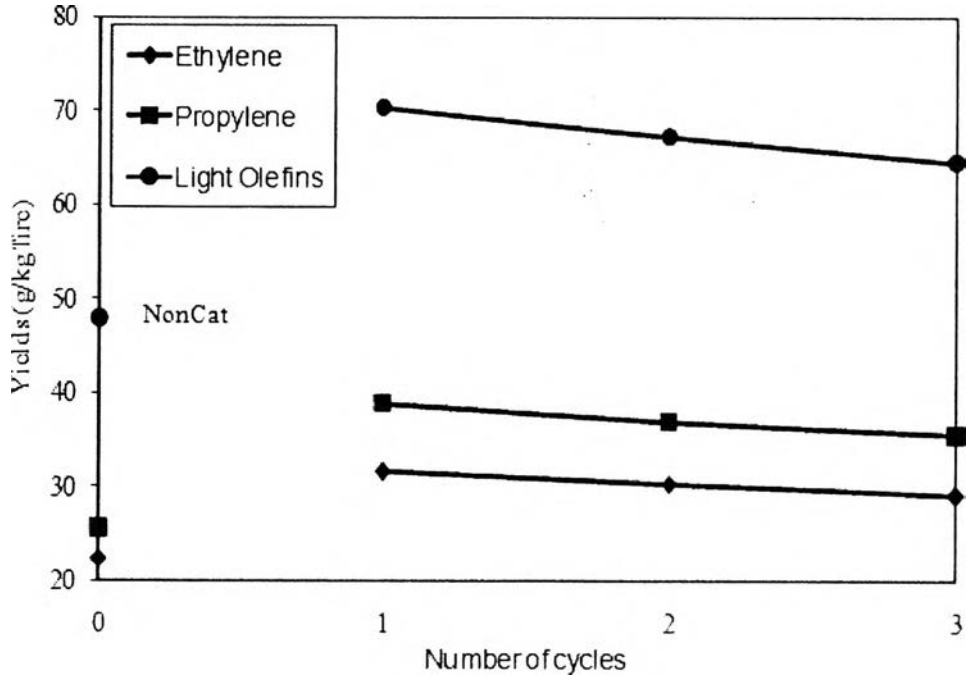

Figure 4.30 Yields of ethylene, propylene, and light olefins obtained from 1 to 3 cycles of operations.

According to Figure 4.31, the main fraction from the catalytic pyrolysis is naphtha. It can be observed that the catalyst reuses from 1 to 3 cycles reduce the naphtha fraction, and consequently increase kerosene, light gas oil, and heavy gas oil. It means that the cracking activity of catalyst decreases with the increasing numbers of reuse. It is because the coke deposits on the active site of the catalysts. Moreover, the quality of oil can be roughly observed from the asphaltene as shown in Figure 4.32. The figure shows that the asphaltene increases with the increasing number of reuse. Due to the coke deposition on the active site of catalyst; therefore, the heavy hydrocarbons are not cracked into the light hydrocarbons.

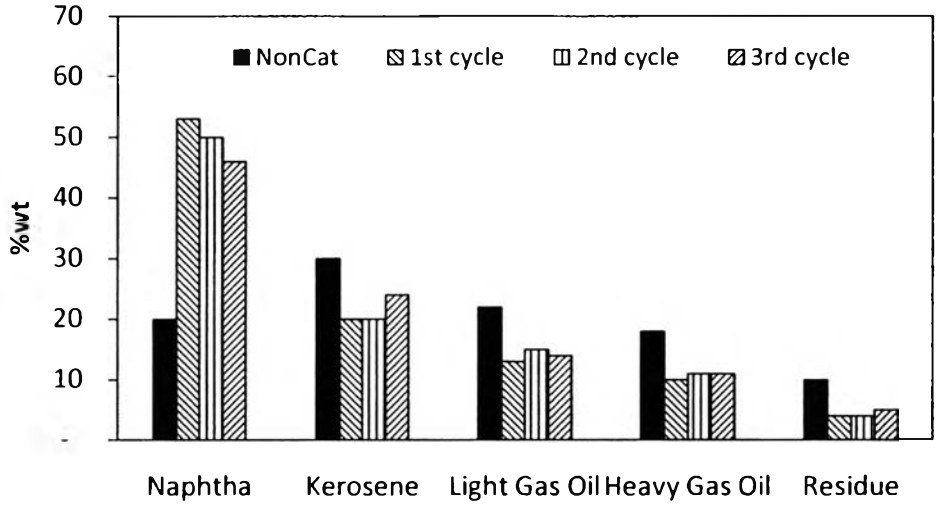

Figure 4.31 Petroleum fractions in the maltenes obtained from 1 to 3 cycles of operations.

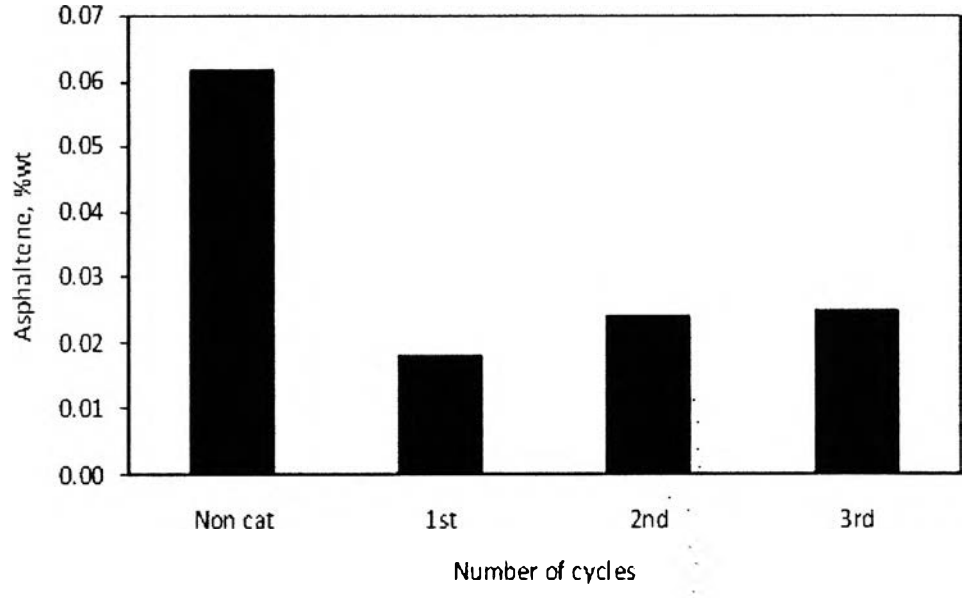

Figure 4.32 Weight percentage of asphaltene in pyrolytic oils obtained from 1 to 3 cycles of operations.

The maltenes were separated into fractions according to the chemical composition using liquid adsorption chromatography. Figure 4.33 demonstrates that the ratio of saturated hydrocarbons to total aromatics slightly decreases with the increasing number of catalyst reuse, which is similar to the ratio of mono-aromatics to total aromatics in Figure 4.34. These results might be described by the loss in the activity of the catalyst due to the coke deposition and metal agglomeration.

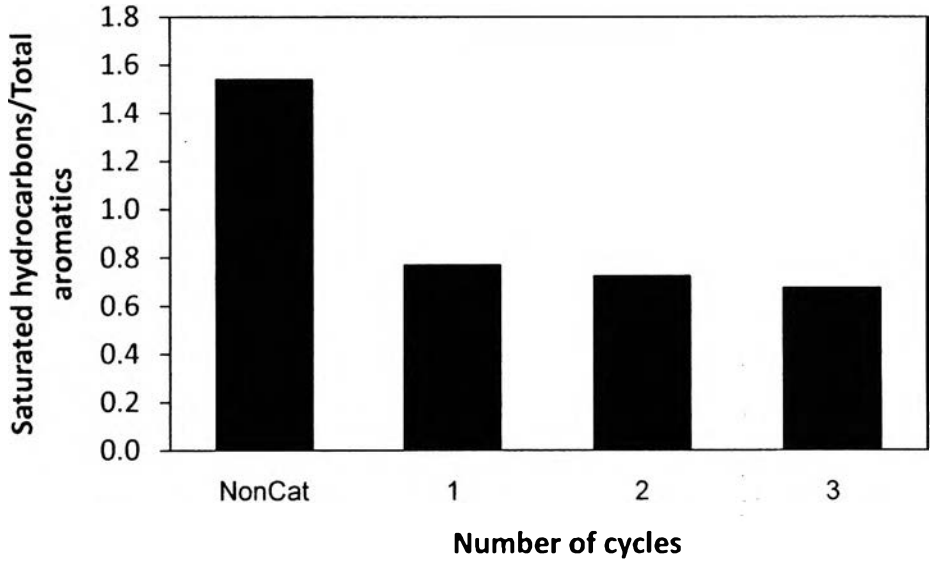

Figure 4.33 The ratio of saturated hydrocarbons to total aromatics in the maltenes obtained from 1 to 3 cycles of operations.

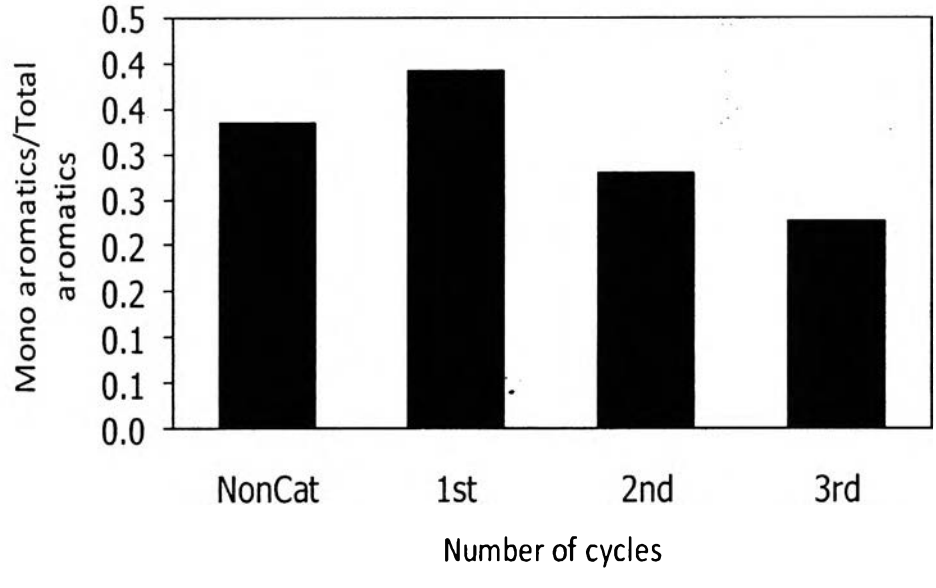

Figure 4.34 The ratio of mono-aromatic to total aromatics in the maltenes obtained from 1 to 3 cycles of operations.

Furthermore, the sulfur content in the derived oil is determined by using the elemental analysis, as shown in Figure 4.35. It can be seen that the sulfur content in the oil product changes insignificantly with the number of cycles.

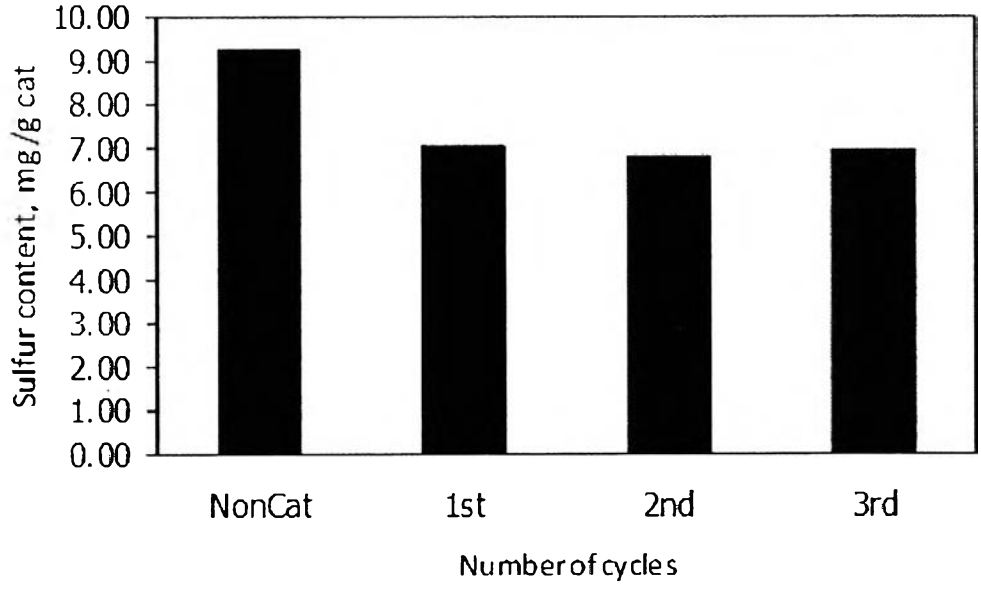

Figure 4.35 Sulfur in the pyrolytic oils obtained from 1 to 3 cycles of operations.

In conclusion, the loss in activity or the activation of catalyst is mainly caused by the coke deposition, the sulfur deposition, and noble metal agglomeration.